EARTH SURFACE PROCESSES AND LANDFORMS
Earth Surf. Process. Landforms (2014)

Published online in Wiley Online Library
(wileyonlinelibrary.com) DOI: 10.1002/esp.3656

A review of terrestrial radar interferometry for measuring surface change in the geosciences

Rafael Caduff,[1,2]* Fritz Schlunegger,[1] Andrew Kos[3,4] and Andreas Wiesmann[2]
[1] Institute for Geological Sciences, University of Berne, Berne, Switzerland
[2] Gamma Remote Sensing AG, Gümligen, Switzerland
[3] Institute for Geotechnical Engineering, ETH Zurich, Zurich, Switzerland
[4] Terrasense Switzerland Ltd, Werdenberg, Switzerland

Received 31 March 2014; Revised 22 August 2014; Accepted 22 September 2014

*Correspondence to: Rafael Caduff, Gamma Remote Sensing AG, Worbstrasse 225, 3073 Gümligen, Switzerland. E-mail: caduff@gamma-rs.ch

ESPL
Earth Surface Processes and Landforms

ABSTRACT: This paper presents a review of the current state of the art in the use of terrestrial radar interferometry for the detection of surface changes related to mass movement. Different hardware-types and acquisition concepts are described, which use either real or synthetic aperture for radar image formation. We present approaches for data processing procedures, paying special attention to the separation of high resolution displacement information from atmospheric phase variations. Recent case studies are used to illustrate applications in terrestrial radar interferometry for change detection. Applications range from detection and quantification of very slow moving (millimeters to centimeters per year) displacements in rock walls from repeat monitoring, to rapid processes resulting in fast displacements (~50 m/yr) acquired during single measurement campaigns with durations of only a few hours. Fast and episodic acting processes such as rockfall and snow avalanches can be assessed qualitatively in the spatial domain by mapping decorrelation caused by those processes. A concluding guide to best practice outlines the necessary preconditions that have to be fulfilled for successful application of the technique, as well as in areas characterized by rapid decorrelation. Empirical data from a Ku-band sensor show the range of temporal decorrelation of different surfaces after more than two years for rock-surfaces and after a few seconds to minutes in vegetated areas during windy conditions. The examples show that the displacement field can be measured for landslides in dense grassland, ice surfaces on flowing glaciers and snowpack creep.

KEYWORDS: terrestrial radar interferometry; mass movements; surface deformation

Introduction

The use of remote sensing methods is increasingly relevant for research and practice particularly when the objective is to accurately detect and measure surface changes in the spatial domain, resulting from mass movements on natural and engineered slopes. In particular, high-resolution spatial and temporal observations can provide an in-depth understanding of the behavior and variability of unstable slopes, and the mechanisms leading to displacement (Schulz *et al.*, 2009). In addition, quantification of surface change has been central to understand the response of mass movements to various triggering factors and has also provided basic information to infer the sediment flux at different spatial and temporal scales, as well as to interpret effects related to coupling relationships between hillslopes and channel networks (Schuerch *et al.*, 2006; Bennett *et al.*, 2012). Since landslides are dominant erosional mechanisms in mountainous terrain (Hovius *et al.*, 1997; Korup and Clague, 2009), detection and measurement of the accompanying surface change is relevant for landslide hazard management.

Quantitative methods applied in the formerly mentioned studies have resulted in point observations with low spatial resolution, and high sub-millimeter accuracy. In contrast, methods such as aerial photogrammetry and airborne laser scanning that are used to survey spatially extensive areas provide large spatial coverage, but the resulting change detection often has accuracies much lower than the results of point surveys. The application of both types of techniques is currently state-of-the art in many fields (Dunnicliff, 1993; Thut, 2009). A third survey technique, offered by satellite synthetic aperture radar (SAR) supports both, a high spatial coverage and in some cases a high resolution and high precision (millimeter-scale) for assessment of surface changes when differential interferometry is used. This method has been applied to quantify surface deformation in response to: tectonic shortening and regional subsidence (Massonnet *et al.*, 1993; Hooper *et al.*, 2012; Tosi *et al.*, 2013), volcanic doming (Lundgren *et al.*, 2004; Jung *et al.*, 2011), landslides and rockslides (Catani *et al.*, 2005; Strozzi *et al.*, 2005; Rott and Nagler, 2006; Calabro *et al.*, 2010; Herrera *et al.*, 2011) and glacial and peri-glacial processes (Mohr *et al.*, 1998; Delaloye *et al.*, 2007; Magnusson *et al.*, 2007; Kääb, 2008). However, there are still substantial limitations to be aware of, such as temporal decorrelation, atmospheric artifacts, phase ambiguity and determination of displacements along line-of-sight (Massonnet and Feigl, 1998; Hanssen, 2001; Colesanti and Wasowski, 2006). In cases where large areas are affected by homogeneous shifts in the surface, non-interferometric image analyses such as intensity- or feature-tracking algorithms may

be applied to calculate the lengths and direction of the displacements. Related applications were presented by Huang and Li (2011) and Nagler *et al.* (2012) where flow lengths and patterns of glaciers were measured, and by Kobayashi (2014) who quantified post-earthquake crustal deformation. Alternatively, limitations of the single techniques can be reduced through the combination of different surveying technologies (Kääb, 2008; Roering *et al.*, 2009).

Over the last few decades, substantial advances have been made in the development of remote sensing technology and methods utilizing terrestrial platforms for change detection. These improvements include the development and application of terrestrial laser scanners (TLSs) (Buckley *et al.*, 2008; Abellán *et al.*, 2009; Jaboyedoff *et al.*, 2012), close range photogrammetry for the generation of high-resolution elevation models (Rieke-Zapp and Nearing, 2005; James and Robson, 2012; Kääb *et al.*, 2014) and vision-based feature tracking methods (Wangensteen *et al.*, 2006; Paar *et al.*, 2012; Travelletti *et al.*, 2012; Kääb *et al.*, 2014).

While the general principle of radar interferometry has not changed since its first implementation (Rosen *et al.*, 2000; Hanssen, 2001), various processing methods have been developed during the past decade, with the scope to reduce the limitations of the technique. These are mainly set by the processing of strongly decorrelated interferograms and can be overcome by point-based coherent scatterer interferometry if coherent points in the scene are present (Colesanti *et al.*, 2003; Werner *et al.*, 2003). Likewise, the detection of atmospheric influences on the radar-wave path (Zebker *et al.*, 1997) resulted in the development of various postprocessing algorithms. Here, the use of independently measured atmospheric data allows for the correction of effects that cause apparent displacements in repeat pass interferograms (Li *et al.*, 2005).

Radar interferometry was originally adapted from space-born platforms to terrestrial applications in order to survey landscapes. This adaptation also allowed the correction of limitations in the technique (e.g. those related to campaign timing and look directions) that are known from satellite SAR interferometry (Rudolf *et al.*, 1999; Reeves *et al.*, 2001; Aguasca *et al.*, 2004; Werner *et al.*, 2008). While satellite-based radar interferometry provides large spatial coverage and high precision for detecting surface change, orbit-related limitations prevent successful operations in some cases. In steep mountainous terrain for example, the effects of radar-overlay and shadowing make reliable interpretation of the interferometric phase difficult (Colesanti and Wasowski, 2006).

Since terrestrial imaging radar systems are designed to operate with very fast revisit times compared to satellite systems, effects related to temporal decorrelation can be significantly reduced. As a consequence, new developments have enabled the quantification of displacement fields of fast decorrelating surfaces with or without very low temporal decorrelation between two acquisitions. Examples include the displacement and surface deformation of ice and snow (Dixon *et al.*, 2012; Wiesmann *et al.*, 2014), fast landslides with grass cover (Del Ventisette *et al.*, 2011b; Caduff *et al.*, 2013) or artificial grass covered dykes prior to breach (Rödelsperger *et al.*, 2013). In addition, recent hardware developments have led to size and weight reduction, making the technology suitable for remote area monitoring (Rödelsperger, 2011; Caduff *et al.*, 2014). Recent reviews of terrestrial SAR sensors are given by Luzi (2010); Rödelsperger (2011) and Monserrat *et al.* (2014). However, the main focus therein lies on a single hardware type or a particular operating system using only synthetic aperture.

In this paper we review the technology and methods currently applied in terrestrial radar interferometry (TRI) in the field of geosciences. The purpose is to present an overview of different terrestrial radar instruments together with interferometric processing and visualization approaches that have been developed over the last decade. Known limitations and the resulting data quality are discussed. We additionally present case studies where Ku-band (17.2 GHz) radar interferometry was applied. Data from those campaigns are used to illustrate measurement and processing strategies for different surface change phenomena. We conclude our paper by presenting possible strategies on how to proceed when planning survey campaigns in different environments. This final section is a synthetic guide to best practice, which focuses on applications based on TRI techniques to quantify a large variety of surface processes.

Principles of Terrestrial Radar Interferometry (TRI)

Terminology and types of instrumentation

A variety of terms are currently used in the literature to describe terrestrial radar interferometric instruments. The most common ones are those utilizing a synthetic aperture technique such as 'Ground-based-SAR' (Gb-SAR) (e.g. Luzi, 2010; Monserrat *et al.*, 2014; or to a lesser extent 'Terrestrial Interferometric SAR' [T-InSAR] for specific interferometric observations [Mazzanti and Brunetti, 2010]). The non-generic nature of the terminology leads to confusion since it does not include real aperture techniques. Although, Rödelsperger *et al.* (2010a) and Lowry *et al.* (2013) used the terms terrestrial microwave interferometry and ground-based interferometric radar respectively, we preferentially assign the generic term 'terrestrial radar interferometry' (TRI) to all forms of phase coherent radar systems used for terrestrial measurements even though non-strictly interferometric measurements are possible as well with the instruments (Monserrat *et al.*, 2013). Likewise, the term TRI additionally represents a complimentary analogy to the terrestrial laser scanning (TLS) technique.

Radar-beams used for the illumination and imaging of areas of interest are formed with different antennas which influence the hardware design. Figure 1 schematically shows the three main radar-acquisition types in TRI that are currently in operation. A dish antenna (in the following sections referred to as Type-I system) produces a narrow pencil shaped beam. A slotted waveguide-antenna (Type-II) forms a very narrow fan-shaped beam in azimuth direction. A third system uses the synthetic aperture of a horn antenna (Type III), whose real aperture produces a relatively wide cone-shaped beam. This system is shifted along a track thereby synthesizing an aperture in the length, where a scatterer is visible from its first to its last appearance. Table I lists the hardware-systems with some of the key specifications that are currently in use for commercial purposes. (Please note that the listed specifications are based on currently available publications and may change as a result of rapid development of the technology.)

Radar image formation and resolution

Imaging radar sensors actively sound the surface of the target area by the emission of a microwave beam formed by a real aperture antenna. The emission of a phase coherent signal is a necessary condition for the interpretation of the differential phase. This adds to the interpretation of the amount of backscatter and the formation of backscatter intensity images. The backscattered and recorded signal therefore represents the

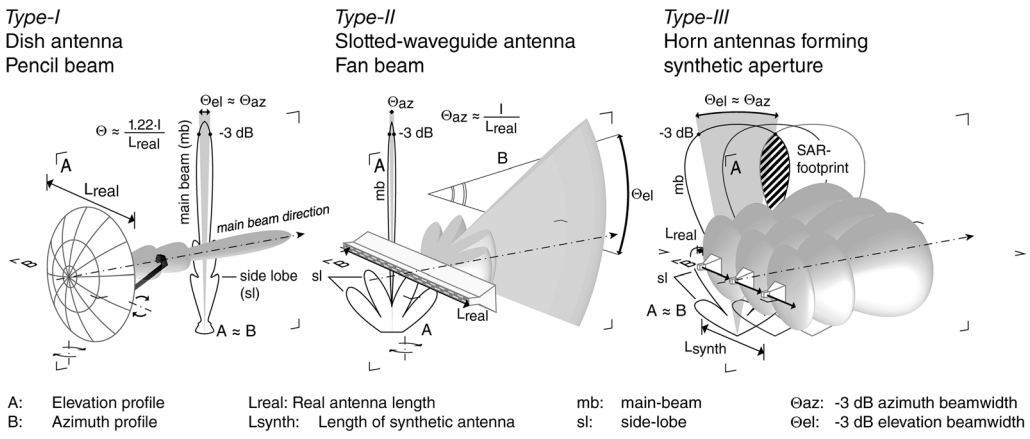

Figure 1. Schematic overview of the three widely used antenna types and their simplified real aperture radiation pattern.

coherent sum of all scatterers in the radar footprint, containing information about the magnitude and phase (Figure 2a).

To obtain a better separation of single scatterers in range, and therefore to increase the resolution, signal emission utilizes a frequency bandwidth. Equation (1) in Figure 3 shows the relationship between frequency bandwidth and slant range resolution. The terrestrial systems use mainly two different techniques: (i) Stepped Frequency (slope stability radar [SSR]: Reeves *et al.*, 2001; LISA: Leva *et al.*, 2003; IBIS: Rödelsperger, 2011) and (ii) Continuous Wave (Gb-SAR: Aguasca *et al.*, 2004; gamma portable radar interferometer [GPRI]: Werner *et al.*, 2012).

To obtain resolution in the azimuth direction, the three most commonly used antenna-types employ different techniques: Type-I systems tilt and rotate the antenna and scan the surface point by point. The Type-II systems rotate the antennas around a vertical axis and collect information line-by-line. The azimuth-resolution of both types depends on the real aperture of the antenna and the range distance of the object according to Equation 2 in Figure 3. Type-III systems shift the antenna along a track and synthesize the aperture. Separation of single scatterers in azimuth requires a computational focusing in this direction. Here, the resolution is given by the length of the synthetic antenna according to Equation 3 in Figure 3. The resulting range and azimuth-resolution values are only nominal if calculated as presented earlier. The actual resolution of the image, that is a combined function of the range and azimuth lines or points, depends largely on the incidence angles to the surface (α, β), as shown in Figure 3 and described by Equations 4 and 5 therein.

The magnitude per single radar resolution cell can be used to form an intensity image. Figure 4 presents an example of an intensity image, which illustrates the backscatter data from an illuminated slope with different coverage types. The backscattering depends on the dielectric properties of the target, target roughness, and the observation geometry (Ulaby *et al.*, 1987). For campaign planning it is important to have a good understanding of the observation geometry including: shadow, overlay, foreshortening and local incidence angles. The backscattering of smooth surfaces, especially at lower incidence angle, is very low and difficult to interpret by means of magnitude and phase. Vegetated areas show a high temporal variability in backscattering. This can be expressed as the ratio between the temporal average and the standard deviation of single observations (I/σ in Figure 4). Regions with a high ratio tend to have a very low (stochastic) variability, which makes them good candidates for point based interferometry (Ferretti *et al.*, 2001; Werner *et al.*, 2003; Hooper *et al.*, 2007).

As previously outlined, the best range resolution is obtained at low incidence angles. However, due to the small radar-footprint, the reflected portion of the signal is also low, especially if the target surface is smooth, resulting in a low signal-to-noise ratio (SNR). In conclusion, the minimum size of a traceable natural object in the radar image depends on the resolution and on the SNR. In reality, however, this does not mean, that objects with size of the radar footprint or larger can be tracked. As shown in Figure 4, an artificial aluminum trihedral corner reflector with a corner length of 20 cm appears as a single dominant scatterer in the scene. Because of its large radar cross-section, the relative contribution of other objects in the same resolution cell is negligible. Therefore, the tracking of objects that are smaller than the nominal resolution is possible if the signal is dominated by this object. Alternatively, the same effect may lead to decorrelation within the resolution cell, e.g. if a dominant scatterer is present in one scene and absent in another one. Because the scattering of natural surfaces is generally very difficult to precisely predict, natural objects that are smaller than the radar-footprint are unlikely to be identified accurately in the image.

Interferometry

The basic principle of interferometry involves the comparison of two radar images where the phase image from one measurement is subtracted from another one. Since the total amount of phase cycles along the line of sight (LOS) between transmitter and scatterer is not known due to phase ambiguities, only relative phase differences are obtained. The process of differential interferometry is shown in Figure 2b.

The ambiguous phase differences of two scenes are the sum of the topographic ($\Delta\varphi_{topo}$), the atmospheric ($\Delta\varphi_{atmo}$), the displacement ($\Delta\varphi_{disp}$) and the system noise ($\Delta\varphi_{noise}$) contribution. Phase differences are usually colored using the interference color spectrum in the range of one wavelength (2π) of the system's center frequency.

For most tasks related to surface change detection and quantification thereof, only the displacement phase contribution ($\Delta\varphi_{disp}$) is of interest. This means, that the other terms have to be identified and subtracted from the total differential interferogram. Compared to space or airborne systems, terrestrial interferometers have the advantage that the antenna-position does not change between two acquisitions (zero-baseline). In this special case the topographic phase contribution ($\Delta\varphi_{topo}$) is zero and can be neglected in most cases. However, for repeat monitoring, errors related to the repositioning of the instrument may occur, which then induces a spatial baseline. In this context, Crosetto *et al.* (2014a) and Monserrat *et al.* (2014) suggest that such a topographic phase can be corrected in the same (or similar) way

Table I. List of most common radar systems and their technical specifications

Device	Type	Radar band	Acquisition time	r_{rg_slant}	r_{az} (@1000 m)	Maximum range	Scene coverage	References	Comments
			(min)	(m)	(m)	(m)	(°hz; °vt)		
MSR	I	X	N/S	N/S	N/S	2500	N/S	www.reutechmining.com Osasan, 2012	
SSR	I	X	25 min per 4000 px	1·5	35	3500	270; 122	Reeves 2001	Given azimuth resolution for 0.9 m diameter dish.
GPRI	II	Ku	10°/sec	0·9	8	10000	360; 35	www.groundprobe.com Werner *et al.*, 2008 Werner *et al.*, 2012	
LISA	III	Ku, C	10–60	3-5	N/S	N/S	20; N/S	Rudolf *et al.*, 1999 Tarchi *et al.*, 2003 Leva *et al.*, 2003	Nominal rail length (lsynth) = 2.8 m
IBIS-L/M	III	Ku	5–10	0·75	4·4	4000	17; 15	Rödelsperger, 2011	Nominal rail length (lsynth = 2.5 m); Scene coverage depends on used antennas
Gb-SAR	III	X	2–3	ns	N/S	N/S	30; N/S	Pipia *et al.*, 2007 Pipia *et al.*, 2008 Aguasca *et al.*, 2004	Data presented only for X-band; system description for L- to Ku-band; maximal rail length (lsynth) = 7 m.
FastGbSAR	III	Ku	<0·2	0·75	4·5	4000	N/S	Rödelsperger *et al.*, 2012	Nominal rail length (lsynth = 2.0 m)

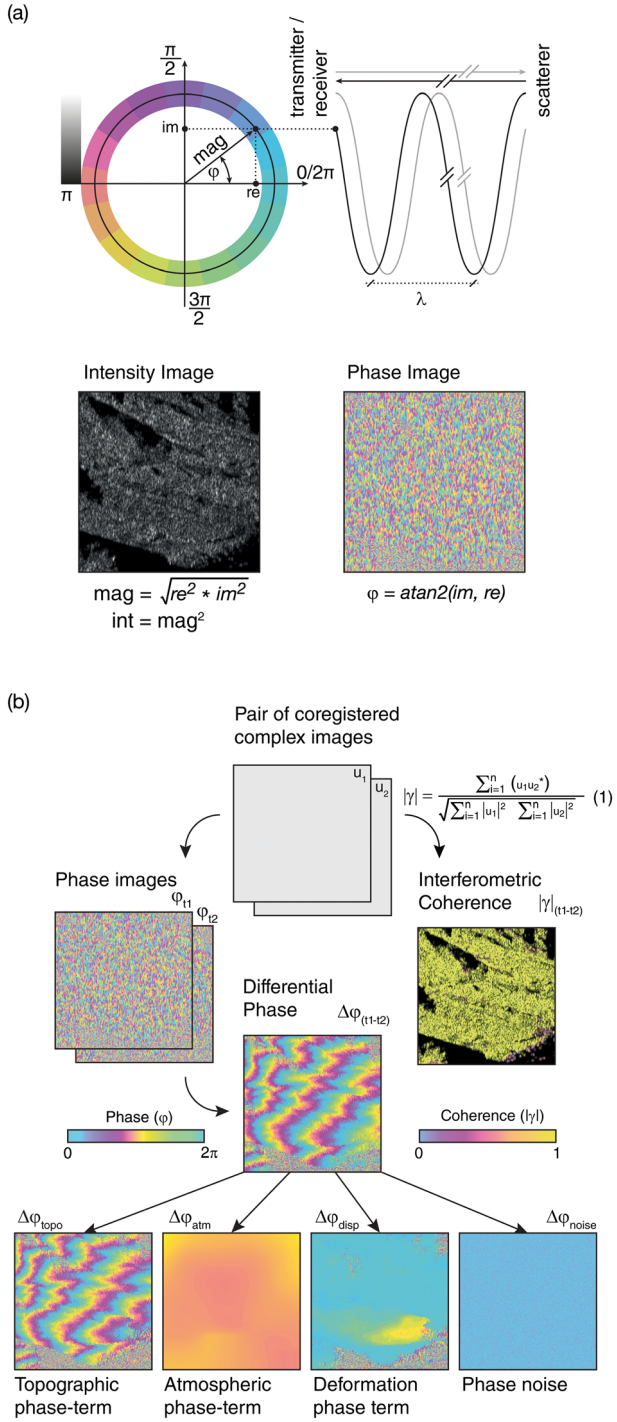

Figure 2. (a) Magnitude/intensity and phase information stored as complex image arrays. Phase coloring is usually done with interference colors ranging from 0 to 2π radians. (b) Phase components of the differential phase and coherence of the interferogram.

as the atmospheric phase ($\Delta\varphi_{atmo}$). However, this only works for small repositioning errors. If these exceed one or several centimeters, then the resulting phase variations can only be corrected with support of a digital elevation model (DEM) of the monitored area. Likewise, in case where this error exceeds the critical baseline, geometric decorrelation may occur as discussed by Zebker and Villasenor (1992) for satellite interferometry.

The remaining phase contributions to be identified are the atmospheric component and the system noise component. Finally the phase has to be unwrapped in order to obtain quantitative values for the displacement phase. For these processing steps, different approaches exist. They are discussed in the following sections.

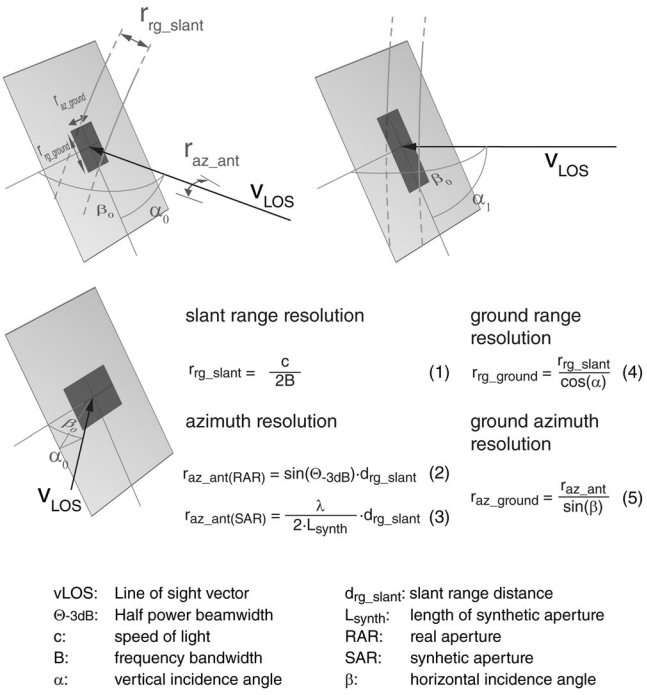

Figure 3. Derivation of ground range and ground azimuth resolution from system slant range and system azimuth resolution.

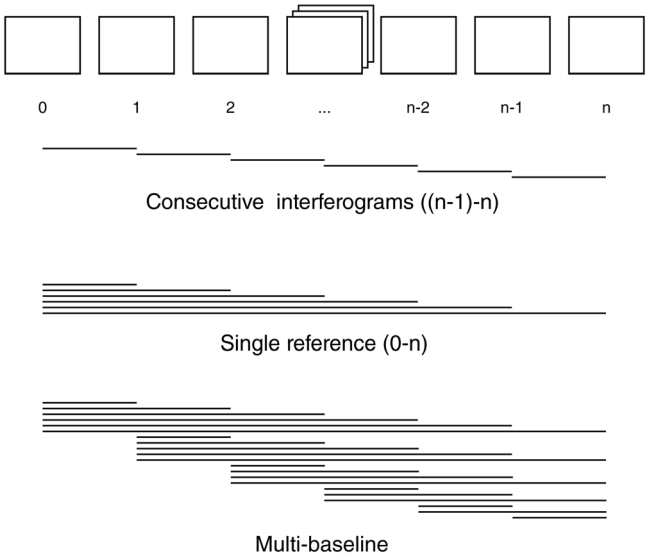

Figure 5. Interferogram processing using different reference scenes (stacking).

Processing strategies for atmosphere removal and noise reduction

Depending on the number of acquisitions, the time-interval in between the acquisitions, the coherence development, the atmospheric phase components and the displacement velocities, different approaches for interferogram generation can be used to separate the phase component caused by the surface displacement from the unwanted effects related to noise and atmospheric perturbations (Figure 5). In general, the processing strategies are adapted from satellite-based interferometric processing.

Changes in air pressure, temperature and humidity induce phase shifts in the interferogram (Goldstein, 1995). In this regard, high radar frequencies show a high sensitivity to atmospheric phase delay (Zebker *et al.*, 1997). In most cases, these perturbations are unwanted since they infer the occurrence

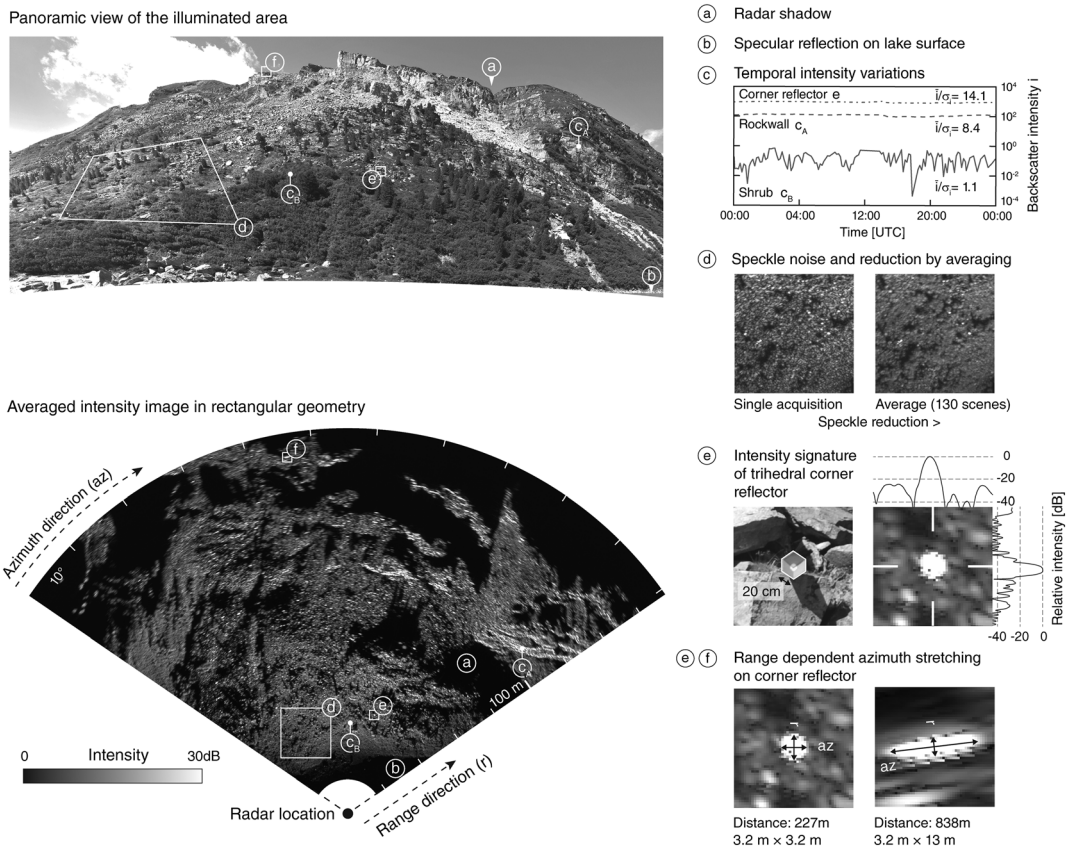

Figure 4. Radar-intensity image and some key-characteristics. Further explanation can be found in the text.

of movements in stable areas or likewise bias the measurement of real displacements. Therefore, the atmospheric- (also referred to as tropospheric-) phase component needs to be satisfactorily removed.

Zebker *et al.* (1997) presented a correction method that is based on a range dependent model where effects related to different temperatures, pressures and water vapor contents are considered as atmospheric artifacts. Fabregas *et al.* (2012) show that in steep topography, height-dependent phase components may be present in the terrestrial radar dataset. In steep mountainous terrain atmospheric effects can contribute to localized, but strong perturbations of the interferograms even for short observation times in the order of minutes (Kristensen *et al.*, 2013; Caduff *et al.*, 2014). Turbulence in the atmosphere are mainly induced by variable radiation caused by differences in solar illumination. In areas where turbulence results in phase shifts, that have a larger spatial extent than the displacement pattern, a simple approach can be applied to remove atmospheric effects. In practice, surfaces that experience a displacement are masked, over which then an interpolation of the phase is applied, as illustrated in Figure 6 for the case of a natural example. Figure 6 also shows modeled range and height-dependent phases for comparison purposes.

Simple normalization using a stable reference point close to the deformed area offers another possibility to reduce atmospheric phase (Kristensen *et al.*, 2013) but often yields non-satisfactory results as shown in Figure 7. Results can be contrasted to those of the masking technique illustrated in Figure 6. Other techniques that allow reduction of atmospheric phase contributions are described in Luzi *et al.* (2004); Noferini *et al.* (2005); Pipia *et al.* (2008) and Rödelsperger *et al.* (2010b).

Alternatively, stacking (or summing up) of multiple interferograms of scenes acquired over a specific time interval offers the possibility of averaging a set of independent interferograms, which results in a significant reduction of phase noise and turbulent atmospheric components (Strozzi *et al.*, 2001). In cases of significant temporal decorrelation, a stack of interferograms with short time intervals can be processed. The single interferograms are then summed in order to determine the displacement time-series. In case of high atmospheric perturbations, a stack with different reference-scenes or time intervals can be generated in order to improve results from atmospheric modeling and correction, analogous to the multi-baseline approach used in satellite SAR differential interferometry (Berardino *et al.*, 2002; Usai, 2002).

However, where a poor spatial distribution of coherent areas yields non-satisfactory results, the methods presented earlier are not sufficient to resolve the displacement pattern from the acquisitions. In such cases, the use of point-wise techniques is more appropriate (Ferretti *et al.*, 2001; Werner *et al.*, 2003; Hooper *et al.*, 2007).

Phase unwrapping

Phase unwrapping techniques are used because of the ambiguous nature of the phase-observation that may exceed one wavelength (2π) in two consecutive observations. In the case of change detection where the surface displacement exceeds π (appears as 2π in the interferogram due to two way-travel of the wave), an interferogram needs to be unwrapped in order to determine the absolute phase (Hanssen, 2001). A conceptual example of errors that result when resolving phase-ambiguities is given in Figure 8. While the relatively long revisit time (Δt) for satellite interferometry inhibits a precise determination of large areas where displacement exceeds π, spatial (two-dimensional, 2D) unwrapping methods were introduced (Goldstein *et al.*, 1988) and later extended in the temporal domain (three-dimensional, 3D) (Hooper and Zebker, 2007). An overview of some spatial phase-unwrapping algorithms is given in Bamler and Hartl (1998).

Errors in the determination of the absolute differential phase can occur in real cases when the displacement exceeds multiple wavelengths in a narrow area, when phase differences per pixel of two neighboring pixels exceed one quarter of a

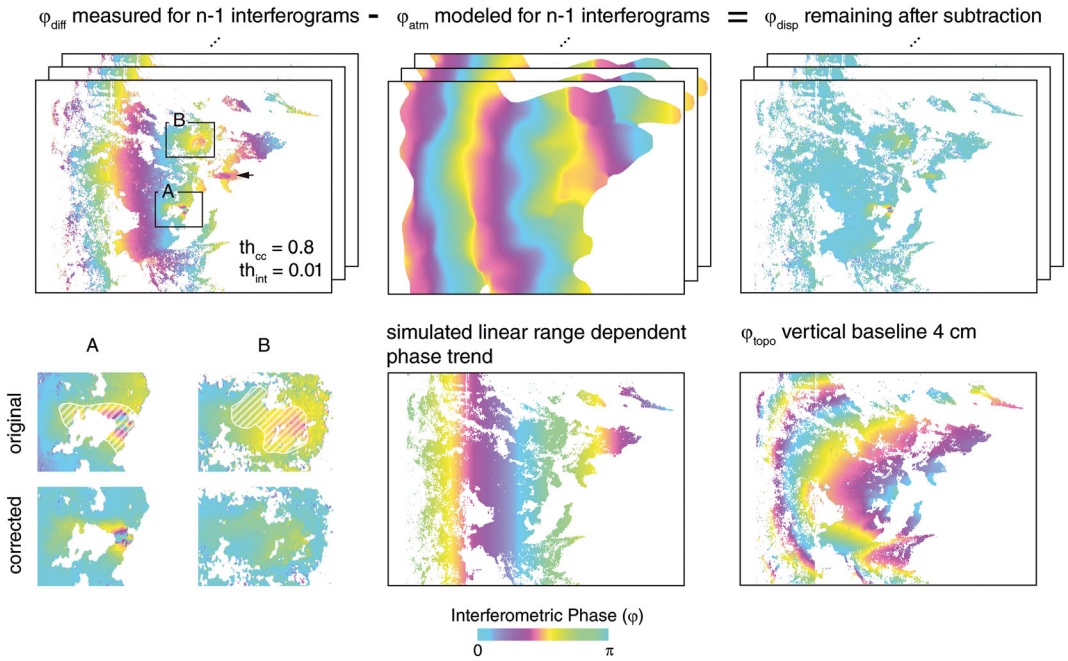

Figure 6. Principle of removing the atmospheric phase component using a supervised approach. Deformation is identified in the unfiltered interferogram (A, B and arrow in the top-left image). Intensity (th_{int}) and coherence (th_{cc}) thresholds are applied, areas showing deformation are masked (bottom-left) and atmospheric influence is modeled (2D) and interpolated over masked areas (top-middle). The modeled phase is then subtracted from the original scene to obtain the deformation phase contribution (top-right and details in bottom left). Bottom middle and bottom right images show the simulated effects of linear range dependent trend and a topographic phase in the same order of magnitude.

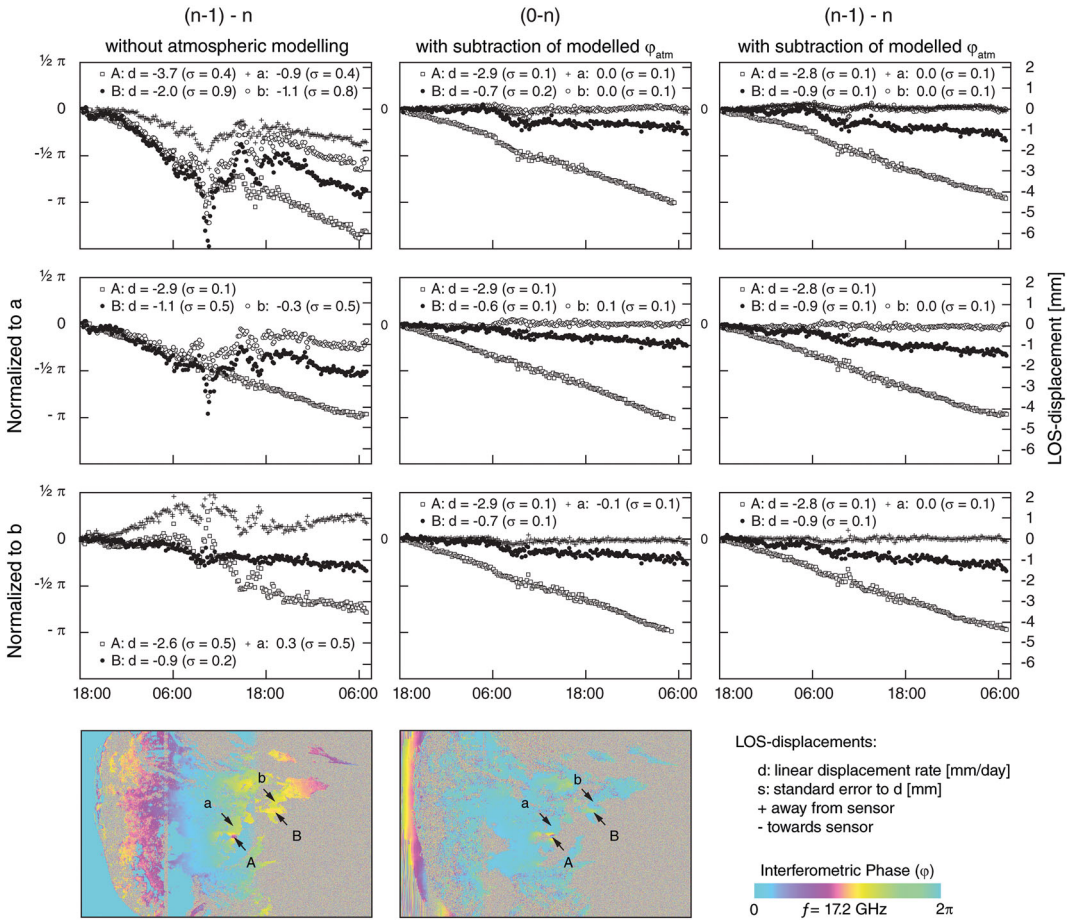

Figure 7. Effects of strategies for atmospheric compensation at sample points in a deformation stack. Left column: Simple normalization to reference points (*a* or *b*). Middle column: Single interferograms to reference scene 0 spatially filtered (according to the strategy presented in Figure 10) and afterwards normalized to *a* or *b*. Right column: Effect on consecutive interferogram, spatially filtered and added to a deformation time series.

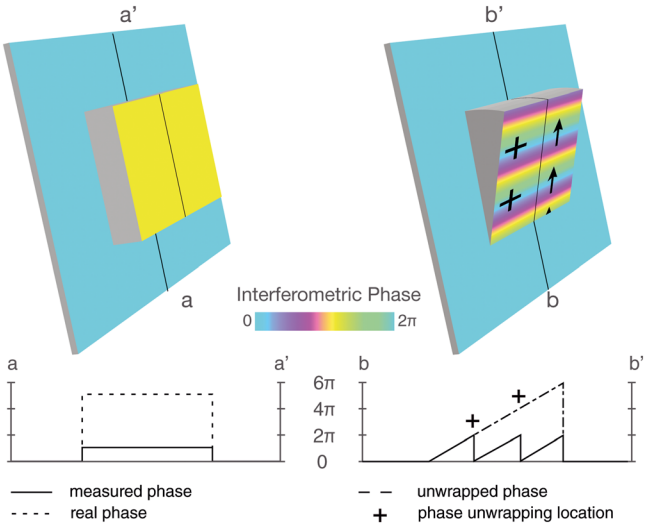

Figure 8. Schematic representation of the spatial unwrapping process. For isolated areas (left) where the total LOS-displacement exceeded 1/4 l, the ambiguous phase cannot be resolved correctly. For tilting processes, absolute displacement can be derived by spatial unwrapping (+) along the indicated arrow direction.

wavelength ($\lambda/4$) (Hanssen, 2001). As a consequence, the fringe visibility and thus the coherence is poor. Figure 9 shows an example where the displacement of a debris-slope front exceeds a multiple of a wavelength between two scenes ($\Delta t = 55$ days). Two coherent areas (*a* and *b*) in the interferogram are separated along a distinct line with low coherence. Phase unwrapping must cross this line in order to determine the correct absolute LOS-displacement values in region *b*, thereby assuming that region *a* was not deformed.

Since the time interval between two measurements can be set very short, the spatial component of phase unwrapping can be neglected if the acquisition interval is far below $\lambda/4$ with respect to the displacement rate. Thus errors in phase unwrapping can be avoided.

Coherence

Quantitative assessment of differential interferograms requires interferometric coherence as the fundamental prerequisite. Coherence is described by Zebker and Villasenor (1992) as result of similar interaction of a scatterer in different acquisitions.

For TRI temporal decorrelation may be significant and is a result of changes in the backscatter characteristics of the surface at the scale of the resolution cell. Decorrelation is invoked by random movement of a single scatterer in the single radar-footprint. It thus depends on the surface cover characteristics and/or the displacement gradient (see also the displacement related decorrelation shown in Figure 9). Fast decorrelation of vegetated areas can appear in a very short time and is mainly caused by wind changing the backscatter intensity (Wegmüller and Werner, 1995; Santoro *et al.*, 2010).

Since the coherence is a qualitative parameter that characterizes the stability at the scale of the ground resolution cell, it can be estimated from the interferometric data using a 2D kernel that is based on Equation (1) in Figure 2b. Loss of coherence can be used to infer large changes in a landscape, for example, land-

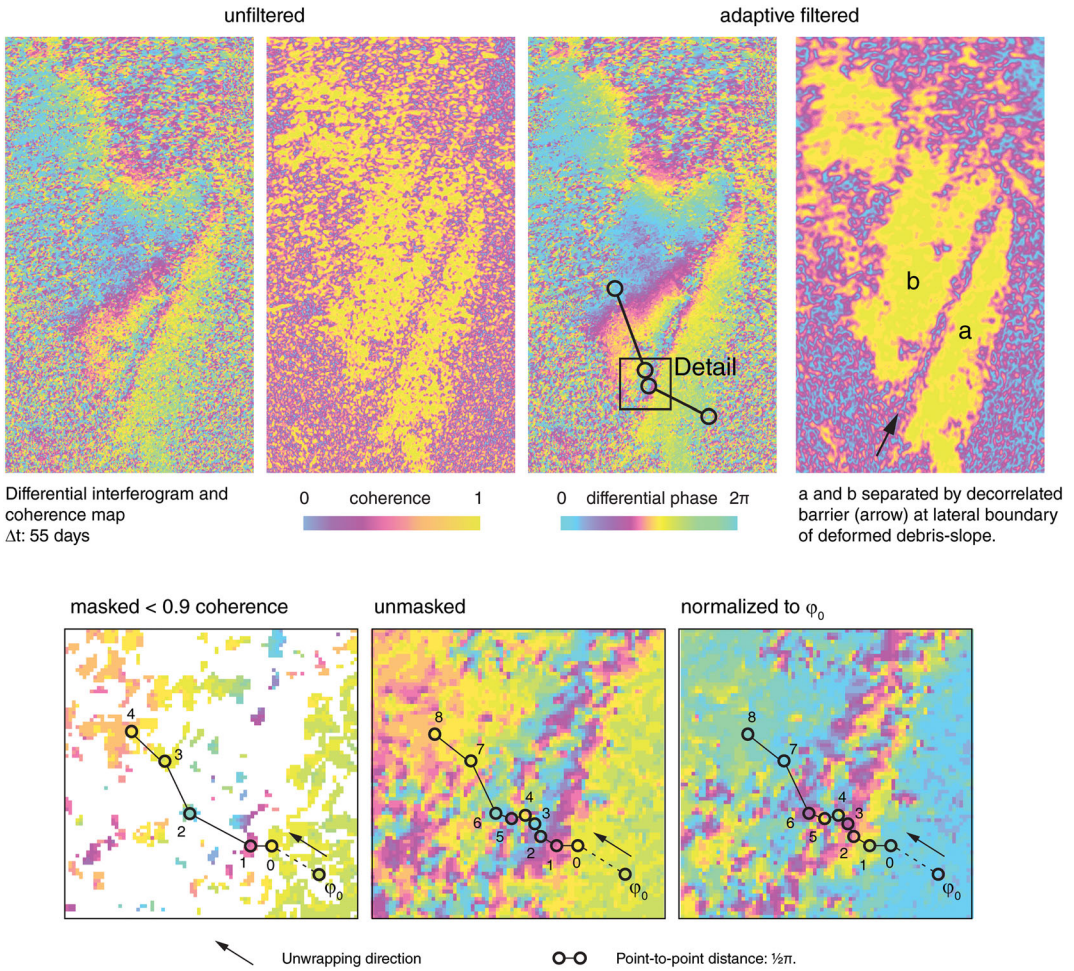

Figure 9. Differential interferogram and coherence of the frontal part of a thrust debris-slope (situation in Figure 12). Strong deformation along the thrust-line causes decorrelation in the long time-interval of the observation. Fringe visibility in this part (detail) is poor and different solutions for the unwrapping are achieved depending on the chosen coherence threshold.

use mapping (Dellepiane *et al.*, 2000; Strozzi *et al.*, 2000; Smith and Askne, 2001; Engdahl and Hyyppä, 2003), mapping of snow avalanches (Martinez-Vazquez and Fortuny-Guasch, 2006; Wiesmann *et al.*, 2014), identification of rock-fall occurrence (Figure 10; Rödelsperger, 2011), and delineation of landslides where displacements exceed several wavelengths of the LOS-displacement, which however, prevents the determination of the absolute displacement (Calabro *et al.*, 2010; Caduff *et al.*, 2014).

In general, images with coherence values above 0.8 are best suited for interferometric processing because the standard deviation (SD) of the phase is $< 10°$. Adaptive filtering methods allow a more precise delineation of areas with different coherence values (Goldstein and Werner, 1998), which in turn, will improve the results of the phase unwrapping. Figure 11 presents a collection of empirically derived data that describes the evolution of the temporal decorrelation at Ku-band for different surface types and various timescales. For instance, decorrelation can occur between acquisition times of a few seconds only. In contrast, images can be characterized by stable coherence even if the acquisition times are more than two years apart.

Precision and LOS sensitivity

The precision of a radar system depends on different variables such as the system frequency, the system noise which reduces the sensitivity of the specific sensor, and system independent terms such as atmospheric conditions. Werner *et al.* (2012) indicate that the sensitivity of a Ku-band sensor (GPRI) with a SNR of 30 dB is equivalent to 0.04 mm deformation. Luzi *et al.* (2004) calculate the sensitivity of the phase measurement of 0.7 mm for a C-band sensor (LISA). In X-band, a sensitivity of ±0.1 mm (SD) for the SSR is given in Harries *et al.* (2009). Usually, the stated values can be interpreted as precision only if the effects of atmospheric perturbation on the phase measurements are absent. These latter effects tend to increase with the distance between instrument and target area. An atmospheric correction that is based on the consideration of either, a nearby stable point, or an area and/or a point with independently constrained displacements, yields a precision down to the millimeter-scale. Averaging over multiple independent interferograms may reduce the phase noise significantly and may lead to a higher precision.

Resulting displacement values represent a one-dimensional component in the line-of-sight (d_{LOS}) of the radar. The latter is a vector component of the total displacement (d_{tot}) and depends on the angle between the two vectors (ϑ):

$$|d_{tot}| = \frac{d_{LOS}}{\cos\vartheta} \quad (1)$$

If the displacement direction is known, the measured LOS-displacement can be converted into a modeled 3D total displacement rate, using Equation (1) as shown in Caduff

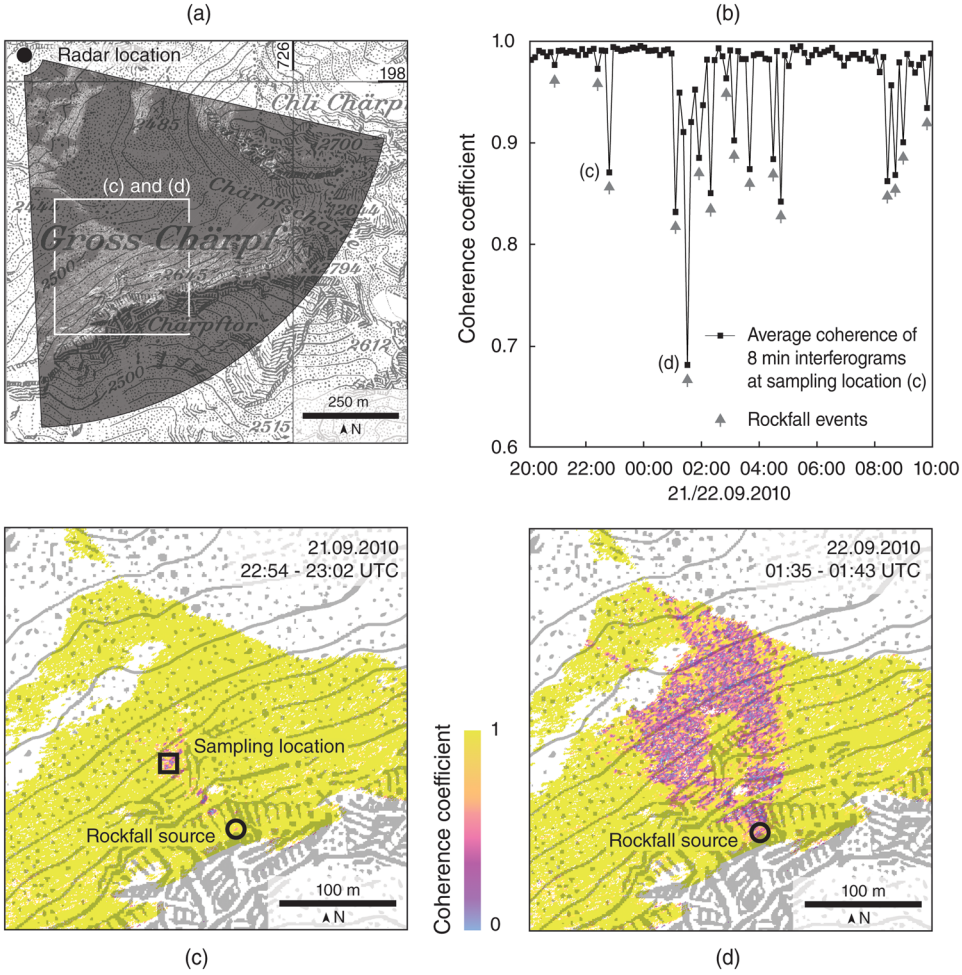

Figure 10. Rockfall detection in a sampling location in the Swiss Alps (a) using coherence maps. Rockfall events are visible as negative peaks in the coherence map of two consecutive acquisitions. Relative magnitude of the events can be assessed by the degree of decorrelation. Decorrelation in this case is induced by disturbing the debris in the initial-, transit-, and deposition-zone by a rockfall event. The affected slope does not inherit any vegetation.

et al. (2014). If the displacement direction is not known a priori, a measurement strategy can be applied where multiple observation points are used for the same target area. This was shown by reconstruction of the 3D displacement field from glaciers that were based on ascending and descending passes of satellites (Mohr *et al.*, 1998). A similar concept can be applied to TRI, where at least two different measurement positions and basic assumptions of the displacement mechanics can be combined to infer a 3D displacement pattern (Severin *et al.*, 2011). For the determination of real 3D displacement fields, the acquisition angles of the LOS axes need to be as perpendicular as possible to each other. Another case of co-temporal acquisition of two active sensors was presented by Kristensen *et al.* (2013).

Non-interferometric analyses

As discussed earlier, interferometric surveys may be limited by strong atmospheric perturbations or by total decorrelation due to very high displacement rates. For satellite SAR time series, intensity information alone can be used to calculate feature offsets that result from surface deformations, which has been documented by several studies (Huang and Li, 2011; Nagler *et al.*, 2012; Kobayashi, 2014). Monserrat *et al.* (2013) and Crosetto *et al.* (2014b) recently showed that intensity-based tracking of artificial corner reflectors may yield information about displacement values in range direction with a precision at the sub-centimeter scale. An application of this technique may be more reliable than e.g. total station measurements, particularly when critical situations (e.g. those prior to slope failure) have to be detected even during weather conditions that are not suitable for total station measurements (e.g. presence of fog).

Georeferencing and visualization

Since Type-II and Type-III systems do not yield direct measurements of the vertical position of a ground resolution cell, real-world coordinates are obtained with a georeferencing approach similar to satellite SAR interferometry, where an independently derived DEM is used as frame (Werner *et al.*, 2002). For steep landscapes such as rock cliffs, the final map resolution is not sufficiently precise to localize the displacements that are identified with TRI. Here, additional surveys with TLS techniques have been useful for the transformation of the radar geometry into the *XYZ*-space (Kos *et al.*, 2011; Tapete *et al.*, 2013). Photogrammetry-based methods offer alternative possibilities to project radar data on high resolution-point clouds, thereby yielding a direct visualization of data on terrestrial images (Caduff and Rieke-Zapp, 2014). Figure 12 summarizes the different possibilities of terrestrial radar data visualization.

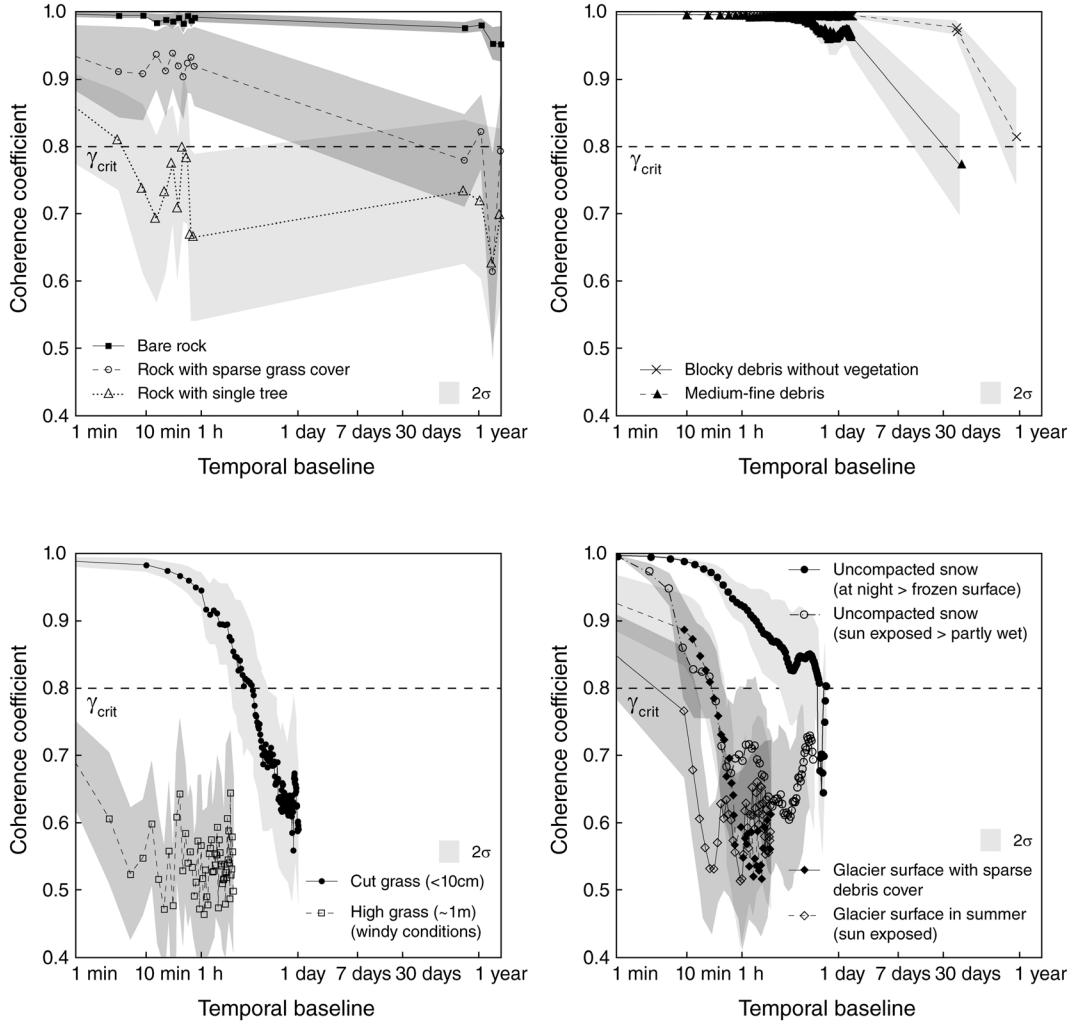

Figure 11. Empirically derived coherence evolution for different surface cover types. Determination of coherence values was done within a 3 × 3 pixel window. Coherence of 100 samples (10 × 10 pixel square area) was averaged. Acquisition was done with a Type-II interferometer (GPRI) operating in Ku-band at 17.2 GHz center frequency.

Recent Applications of TRI for Measuring Surface Change in the Geosciences

In the past decade, TRI has been extensively tested and applied in different research fields (Table II). The applications cover the entire spectrum ranging from displacement measurements of landslide or rockslide related processes, rock slope monitoring, failure modeling and surface changes of glaciers and snow.

From the survey of rock slopes and rockslides towards hazard assessment and early warning

Since temporal decorrelation can severely affect the outcomes of differential interferometry, TRI has been preferentially applied to survey coherent surfaces such as bare rock or constructions in urban environments. TRI has therefore been successfully used in open pit mining environments for hazard assessment and early warning of slope failures (Reeves *et al.*, 2000; Harries *et al.*, 2006; Eberhardt *et al.*, 2008; Harries *et al.*, 2009; Severin *et al.*, 2011; Osasan, 2012; Agliardi *et al.*, 2013). The need for monitoring the stability of rock walls in open pit mines promoted the development of Type-I instruments where they have been designed to be robust and reliable in the harsh working environment of a mine. The instrument robustness ensures stability in autonomous data-collection and processing. Apart from the papers mentioned earlier, only a few additional scientific publications are available, and most of them focus on the success of slope-failure predictions in open pit mines (Table II). In this context, the implementation of real- or near-real-time processing methods for the fast detection and quantification of deformation has been a precondition for successful and timely predictions of landslide failure. An example of a near-real-time processing method using persistent scatterer networks is described by Rödelsperger (2011).

TRI has also been used to survey natural slopes where the surface deformation has been driven by landslides and rockslides processes. The most common application for TRI is the survey of landslides and unstable rock slopes where results support hazard management (Tarchi *et al.*, 2005; Gigli *et al.*, 2011; Kristensen *et al.*, 2013). In this context, long-term continuous monitoring campaigns with TRI together with conventional monitoring techniques yielded in an improved understanding of landslide kinematics (Barla *et al.*, 2010; Crosta *et al.*, 2013) and triggering factors (Herrera *et al.*, 2009; Del Ventisette *et al.*, 2011a; Intrieri *et al.*, 2013). The methodology has not been as frequently applied as conventional monitoring methods because of the relatively high instrument costs and in some cases reflects uncertainty in obtaining desired results due to decorrelation (Michoud *et al.*, 2013). However, in view of the most recent technical developments, and considering the improvements in data processing, we anticipate that the technique will find a wider application in the future.

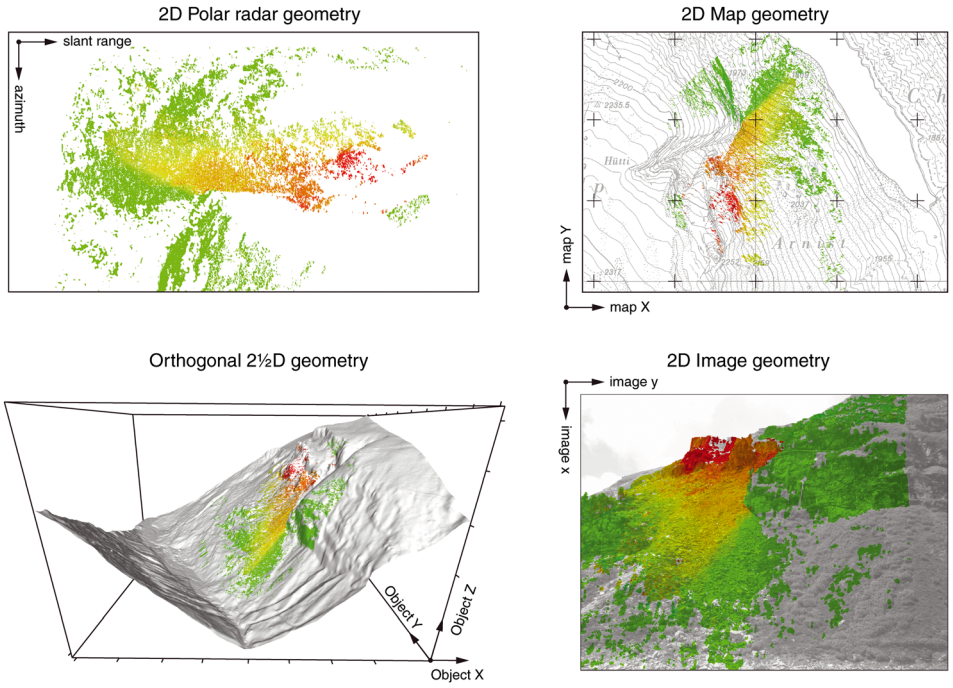

Figure 12. Possibilities for the visualization of the final radar data product (example here: color coded deformation map).

For analysis of the potential failure of rock slope instabilities, a repeat measurement strategy may be sufficient when displacement rates are as low as a few millimeters per year. Type-II and Type-III instruments have proven to be ideal equipment for this purpose because they can be placed exactly in the same position and configured after removal (Noferini *et al.*, 2008; Kos *et al.*, 2013; Crosetto *et al.*, 2014a). For the Type-II system, Kos *et al.* (2013) selected a setup which was based on a common geodetic ground point. A ground-point based reposition control has shown a high accuracy for long-term repeat observations. For repeat monitoring campaigns that include time lags of several months and up to years, it is important that the interferometric coherence of the targeted area remains high. Crosetto *et al.* (2014b) show that in a vegetated slope, only artificial targets (corner reflectors) yield coherent information. In this case where the point density is low and the point distribution over the scene is poor, problems will arise upon phase unwrapping and removal of the atmospheric phase. In the case outlined by Crosetto *et al.* (2014b), maximum displacements measured between two observations were very close to $\lambda/2$ of the instrument, yielding results with high uncertainty due to phase ambiguity. Without redundant measurements or the support of algorithms that allow the estimations of the initial deformation, an absolute determination of the deformation is not possible.

The use of a strategy where landslides and unstable rock slopes are repeatedly monitored, however, offers the possibility to detect small velocity changes relatively early. It also allows precise delineation of unstable rock masses that are prone to failure. Likewise, the same approach can be selected to detect: (i) sites of spontaneous mass movements such as rockfall and blockfall processes that have occurred between two measurements, (ii) locations where surface deformation has not been expected, and (iii) areas where the deformation rates exceed the $\lambda/4$-criterion by a multiple of λ. Although local decorrelation may prevent the quantification of the displacements in these cases, the categorization of sites experiencing deformation may be used qualitatively for the interpretation and mapping of relevant phenomena and processes (Rödelsperger, 2011; Caduff *et al.*, 2014).

Displacement field measurements on fast decorrelating surfaces: landslides, glacier flow, snow creep

Recent tests on slopes with potentially fast decorrelating scatterers, for example dense grass, showed that mapping and quantification of surface displacement is possible with Ku-band sensors when acquisition intervals are adjusted accordingly (below the decorrelation time of the surface: Figure 11) to prevent single scene decorrelation (Caduff *et al.*, 2013; Rödelsperger *et al.*, 2013). Fast temporal decorrelation may also occur when surveying ice-covered surfaces (Figure 10). Even though glacier flow is an ideal candidate to be measured with TRI because of the large extent of the area experiencing displacement and the relatively high flow velocity, only few campaigns have been reported in the literature up to now.

Harries *et al.* (2009) who applied a Type-I system in a mine and observed areas covered by ice. Unfortunately no further details are given here, except that surveys that were carried out during the daytime yielded noisy results. They were related to changes of the ice surface e.g. in response to ice melting. Therefore, surveys of glacier surfaces are more successful if carried out during nighttime. Measurement results at the outlet of a calving glacier showed the feasibility of deformation measurements where the displacement velocities were a few meters per day. This has recently been documented by Dixon *et al.* (2012) who acquired data with intervals of several minutes with a Type-II system.

In the same context, positive results with campaigns were reported by Luzi *et al.* (2007) and Noferini *et al.* (2009) who used Type-III systems to measure the surface deformation of the Belvedere Glacier south of the Monte Rosa where a dense cover by rock debris resulted in a high coherence. However, the fast change of the surface during the snow melting period precluded the identification and delineation of the various processes contributing to the displacement of the surface. In contrast, however, such a task was successively achieved for the surface of the Gorner-Glacier in Switzerland with a Type-II instrument. This testifies the suitability of radar interferometry techniques to monitor changes of the surface of a glacier during its demise in relation to down-melting processes (Riesen *et al.*, 2011).

Table II. Selected recent publications of terrestrial radar interferometry (TRI) applications

Rock mass instabilities	d_{LOS}/day	Band (Type)	Surface cover	Summary
Tarchi *et al.* (2005)	maximum 30 mm	Ku (III)	Rockslide debris and outcropping rock surrounded by forest	After the release of a disastrous rock slide, a terrestrial radar interferometer was used during a continuous campaign to localize and quantify ongoing surface displacement. A general deceleration was detected. The study demonstrated the applicability of TRI as an operational tool for early warning in emergency situations.
Gischig *et al.* (2009)	0·05 mm	Ku (III)	Natural steep rock and debris slope	Five repeat surveys of the Randa rockslide in a timespan of two years revealed the location of discrete active release planes that are consistent with field observations and LiDAR results.
Harries *et al.* (2009)	—[a]	[X] (I)	Artificial rock and debris slopes, partially covered with snow and ice	Case studies for the use of radar interferometry for slope stability assessment for open pit mining are described. Detection of acceleration phases of rockslope instabilities lead to reduction of economic and health risk within the mining process by early evacuation of workers. Difficulties in detecting small rock slope deformations during periods of heavy snowfall or if the rock slope is covered with snow and ice were stated. Possibilities of monitoring glacier movement and in detecting avalanches were concluded.
Gigli *et al.* (2011)	10·6 mm	— (III)	Natural rock slope partly with debris and vegetation	A study of a rockslide in a natural rockslope. A terrestrial radar campaign was applied prior to main slope failure. TRI was combined with geophysical measurements to characterize the extent and to estimate the affected volume.
Severin *et al.* (2011)	27·5 cm	[Ku][b] (III)	Engineered rock wall of open pit mine	The deformation of a rockwall in an open pit mine was assessed by simultaneous monitoring from two different positions. LOS displacements for points visible from both positions were converted to 3D displacement vectors by assuming deformation rates in the cross direction.
Agliardi *et al.* (2013)	0·2–7·5 mm	[Ku] (III)	Artificial rock slope in fractured rock, partially debris covered	Magnitude and sliding mechanisms of a rockslide in a quarry were studied using TRI. In combination with TLS and numerical modeling, structural control of the deformation events was concluded. TRI revealed seasonality of deformation rates (slower in winter and spring).
Crosta *et al.* (2013)	> 4,3 mm	— (III)	Rock, bare soil and debris within forest	Continuous monitoring of the La Saxe rockslide (Italy) led to the determination of the spatio-temporal evolution of the deformation and thus to the zonation of the landslide. The zonation was used to generate a one-dimensional block model that allowed forecast of displacement behavior as a result of changing hydrogeological conditions.
Intrieri *et al.* (2013)	—	[Ku] (III)	cinder, lapilli, scoriae, pieces of lava	The combination of displacement information derived from TRI with a variety of independent observations led to a linkage between landsliding and the rise of magma in a volcanic environment.
Kristensen *et al.* (2013)	maximum 0·125 mm	Ku (III)	Mostly outcropping rock and debris; vegetation at lower slope.	A monitoring of surface displacement at the Åknes rockslide was performed over a five year period using a repeat-continuous monitoring approach. A comparison was made to total station measurement and satellite InSAR using Radarsat-2 acquisition. In 2012, two radar instruments were used to acquire simultaneously from different look directions.
Caduff *et al.* (2014)	2 mm	Ku (II)	Bare soil / highly fractured rock	The headwater of a steep alpine debris flow catchment was monitored with real aperture radar. Continuous deformation was detected within a few hours. Three repeat measurements were taken in one year. Measured LOS rates were converted to 3D displacement rates assuming homogeneous deformation based on geological observations. Turbulent atmospheric effects were detected and related to differences in solar illumination.

(*Continues*)

Table II. (Continued)

Rockfall/blockfall	d_{LOS}/day	Band (Type)	Surface cover	Summary
Harries *et al.* (2006)	—	[X] (I)	Artificial rock and debris slope	Two examples are presented where pixel size deformation was detected. This was related to rock and blockfall events in an open-pit mine. Rapid acceleration within hours led to evacuation of personnel and equipment one hour prior to failure.
Kos *et al.* (2013)	0·02 mm	Ku (II)	Nearly vertical rock-face	A case study where a discrete rock slab was monitored during a five month period with three repeat measurements is presented. Deformation mechanisms of toppling and buckling were detected. The extent of the deformed area could be identified with coherent phase information.
Rödelsperger (2011)	N/A	Ku (III)	Debris slope rock outcrops and tree cover	An example is shown, where rockfall events were detected using an interpretation of phase noise. Timing, source location and relative magnitude of the events could be determined.
Landslides	d_{LOS}/day	Band (Type)	Surface cover	Summary
Herrera *et al.* (2009)	maximum 13 mm	C (III)	Low pasture with sparse blocky debris	Combined observations of differential global positioning system (DGPS), inclinometer and TRI showed acceleration phases linked to rainfall events with high intensity. The radar measurements were further used for the back analysis of deformation using a one dimensional infinite model.
Barla *et al.* (2010)	maximum 0·37 mm	Ku (III)	Coherent areas above tree line; mainly rock and debris	A 121 day long continuous monitoring campaign at the Beauregard landslide (Italy), located above an artificial hydropower lake and arch dam, led to the detection of surface movement in the upper part of the slope. This information was used to enhance the kinematic model based on different surface and subsurface monitoring techniques.
Del Ventisette *et al.* (2011a)	maximum 7 mm	Ku (III)	Soil and rock exposed along scarps within forested area.	This paper presents results of a continuous landslide monitoring that was accomplished during one year period. Changes in displacement rates were compared with meteorological data. A link between rainfall intensity and displacement rate change was identified.
Caduff *et al.* (2013)	1·5–40 cm	Ku (II)	Dense grass / pasture	Conventional 2d-interferometry in densely grass covered slope from a slant range distance of up to 7 km (deformation area 3.1–3.8 km) was shown to be feasible when surveyed with a real aperture Ku-band sensor. Maximum LOS displacement of 40 cm/day was detected in a five hour campaign. Displacement rates decreased three weeks later to maximum 10 cm/day. The results of the second campaign were verified with total station measurements of artificial corner reflectors.
Lowry *et al.* (2013)	3–18 mm	Ku (II)	[Bare soil on active landfill, sparse dry vegetation]	Monitoring of a landslide in an artificial landfill was made with real aperture sensor. The daily displacement rates retrieved from two continuous campaigns were compared to DGPS measurements.
Monserrat *et al.* (2013)	max 1·4 mm	Ku (III)	Artificial targets (corner reflectors)	A non-interferometric approach for the displacement determination, using only intensity information from the terrestrial radar, is shown at the Vallcebre-landslide (Spain). Errors of measured displacement at 15 corner reflectors were between 0.03–5.48 cm
Glacial and peri-glacial environment	d_{LOS}/day	Band (Type)	Surface cover	Summary
Noferini *et al.* (2009)	~10 cm	C (III)	Debris covered glacier tongue	Glacier movements were continuously monitored during one month. Velocity maps obtained by differential phase are shown. A DEM was generated from the data and compared to the topography that was dated two years before the study.
Strozzi *et al.* (2009)	2·5 –40 cm	Ku (II)	Debris and rock-slope	Two rock glaciers in the Swiss Alps were observed with a set of satellite SAR interferometry observations and TRI. The study also shows the

(*Continues*)

Table II. (Continued)

				potential of TRI to map continuously and fast deforming (permafrost) areas and to fill the large gap between revisit times of the currently available satellite-based sensors.
Riesen *et al.* (2011)	~25 cm	Ku (II)	Glacier ice, partially covered with moraine debris.	Over a four day period the surface ice motion was monitored with TRI. Changes in rates could be detected during drainage of a nearby glacial lake. Rates were compared to additional measurements with total station and GPS.
Springman *et al.* (2012)	2 cm	Ku (II)	Debris (block-glacier)	An example is presented where the direct assessment of surface deformation of a block-glacier with TRI was shown. The technique is discussed within a multidisciplinary framework with the goal of understanding alpine permafrost response to environment changes.
Voytenko *et al.* (2012)	3·7 m	Ku (II)	Glacier ice	The study showed radar interferometry is capable of measuring the rapid flow of a calving glacier up to a distance of 6.5 km. Velocity data were compared with TerraSAR-X data. The study illustrated a presence of high spatial and temporal variability of glacier flow velocities.
Snow	d_{LOS}/day	Band (Type)	Surface cover	Summary
Martinez-Vazquez and Fortuny-Guasch (2008)	N/A	C (III)		An algorithm of automatic detection of snow avalanche events is presented, which is based on the spatial decorrelation signatures of such events. Results of six winter campaigns are presented and a performance analysis is given.
Luzi *et al.* (2009)	N/A	C, S (III)	Snow slope during snow accumulation phase	This experimental study shows the potential of snow depth change monitoring during snowfall using the differential phase. The dual frequency study showed reduced coherence loss with time, using lower frequency.
Wiesmann *et al.* (2014)	$>$ 12 cm	Ku (II)	Natural snow and skiing slope (mechanically compacted)	This study shows an example, where it was possible to measure deformation rates of creeping snow in an alpine skiing resort. Diurnal observations yielded displacement rates in the order of $>$ 12 cm per day. Decorrelation effects within 1–3 minutes could be observed as result of skiing activity. Slopes with different aspects show different backscatter intensity changes.

[a]No information available.
[b]Not explicitly mentioned in the paper. The information is taken from the provider of the system.

Interferometric measurements on snow slopes may reveal significant insight into the properties of snow and mechanisms leading to displacement and failure. For example, snow accumulation was determined with a dual-band (C- and S-Band) system (Luzi *et al.*, 2009). Another study showed the feasibility of the automated detection and mapping of snow avalanches by analyzing decorrelation in a pair of consecutive interferograms prior and after the avalanche was released (Martinez-Vazquez and Fortuny-Guasch, 2008). The only example so far of direct assessment of the displacement of the snowpack due to snow-creep is given by Wiesmann *et al.* (2014). A displacement map of this campaign is shown in Figure 13 revealing local snow creep in the maximum order of decimeters per day.

Generation of DEMs with TRI

An alternative application of terrestrial radar interferometers is the generation of a topographic surface model using the topographic phase signature (Nico *et al.*, 2005; Noferini *et al.*, 2007; Rödelsperger *et al.*, 2010b; Strozzi *et al.*, 2011). Instruments can be modified to induce a defined vertical baseline of a few centimeters to decimeters. Comparisons with independently retrieved elevation models showed that the heights were relatively accurate as they deviated from the standard elevations in the range between 0.8 and 3 m (Rödelsperger *et al.*, 2010b), 3 m (Strozzi *et al.*, 2011) and around 5 m (Nico *et al.*, 2005; Noferini *et al.*, 2007). These accuracies are good enough to quantify large changes in the surface topography, but they are worse than those of LiDAR measurements (Abellán *et al.*, 2009; Jaboyedoff *et al.*, 2012).

Guide to Best Practice for the Application of Terrestrial Interferometry

A terrestrial radar campaign must be properly designed, in order to obtain the desired results. The main factors that need to be considered include the assessment of, setup geometry of the measurement device, surface cover to be measured, and local atmospheric effects as these will have a direct influence on the results. In this section, we synthesize the salient points of this review combined with our knowledge about the current state of the technique (including the results of past surveys described in previous sections) in the form of a guide for best

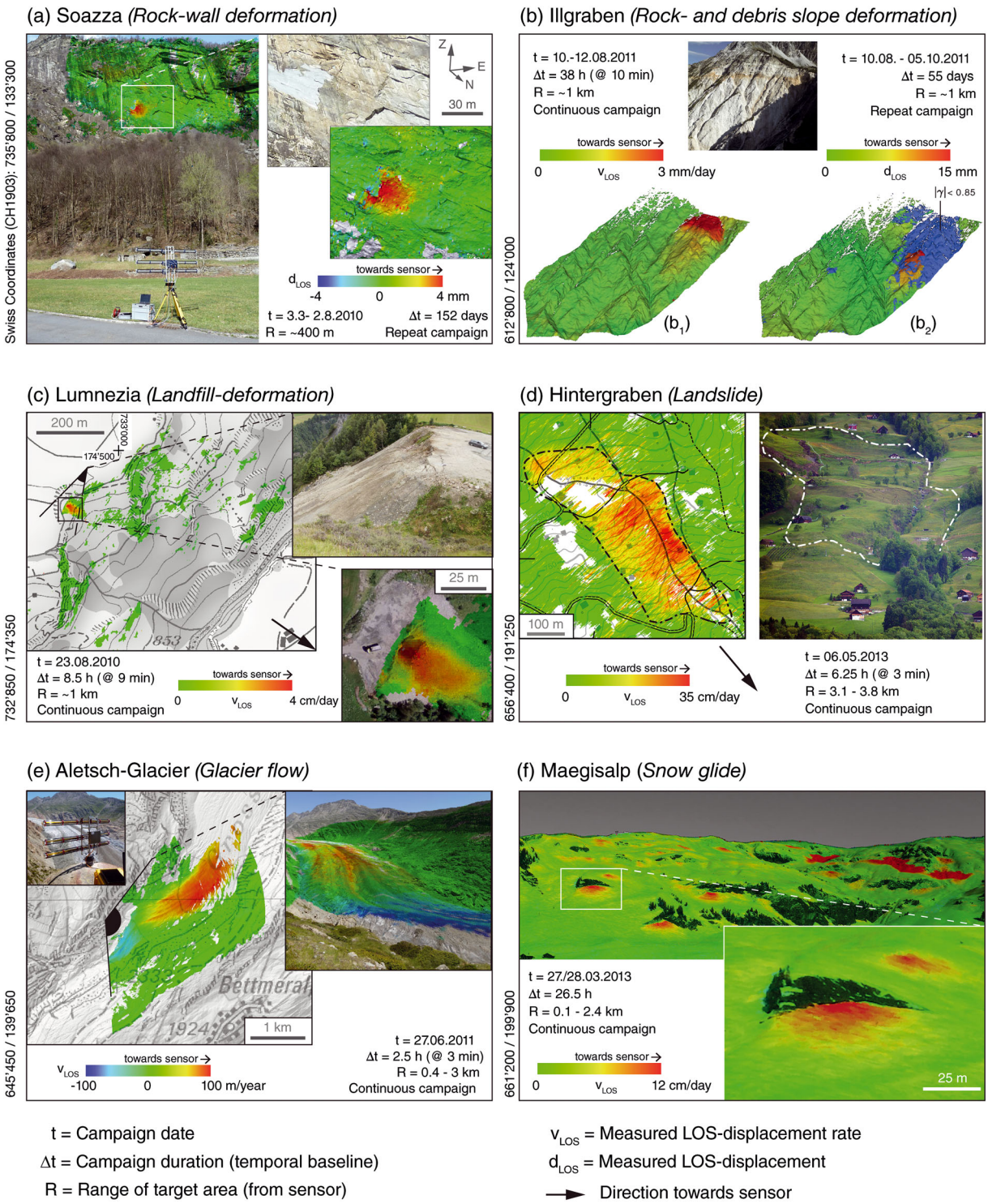

Figure 13. Examples of deformation measurement campaigns where surface cover types and deformation rates are different. Surveys were accomplished with the gamma portable radar interferometer (GPRI) at 17.2 GHz. Further information on the single case studies can be taken from: (a) Kos *et al.* (2013); (b) Caduff *et al.* (2014); (d) Caduff *et al.* (2013); (f) Wiesmann *et al.* (2014).

practice. The guide is intended as an aid for the planning and execution of successful field campaigns.

In order to detect and quantify surface changes satisfactorily, the following points must carefully be considered in the planning of a campaign:

(a) Visibility of the target area
(b) Surface cover of the area of interest
(c) Displacement field including rates and mechanisms
(d) View geometry to expected LOS
(e) Radar resolution and SNR
(f) Atmospheric influences
(g) Technical constraints (hardware, setup, etc.)

(a) *Visibility* not only concerns the effective visibility of the area of interest but also addresses an important point for interferometric processing where the correlation of images is crucial. An unfavorable distribution of image patches (e.g. 'islands') can have the effect that the displacement signal cannot be separated properly from the atmospheric phase. Also, a possible disconnection can lead to

unwrapping ambiguities to the extent that the displacement cannot be quantified properly (Figure 9).

(b) The modality of the *surface cover* in the target area defines the nature of the scatterer. A high precision assessment of the surface's displacement field using differential phase requires the maximum possible number/percentage of coherent scatterers. Figure 10 shows how the coherence of different surface cover types changes with time. The pattern illustrated in Figure 10 is based on empirical assessments and can differ from case-to-case. However, an accurate prediction of the temporal decorrelation requires direct on-site measurements with the pre-specified sensor and radar-frequency. Generally, it can be said that in forested areas, the displacement phase of the terrain surface cannot be retrieved with the sensors described in this review. For other surface covers, acquisition intervals have to be adjusted in order to minimize the temporal decorrelation. Figure 14 shows a rough estimation of the decorrelation time for different surface coverage. It also illustrates the potential applicability for the detection of displacements with different velocities at Ku-band, and it includes estimations of how disturbances of the surface such as soil erosion (e.g. in response to a heavy rainstorm) can lead to decorrelation, thereby precluding the detection of very slow displacements due to absent phase stability.
Although the installation of coherent targets (e.g. metal corner reflectors in the target area) overcomes some of the problems stated earlier, the added value in comparison with other point-based observation methods needs to be carefully considered. Nevertheless, the displacement of the corner reflectors can be measured by radar instruments even at foggy or cloudy conditions, when optical instruments (e.g. total station) do not return results.

(c) Not only the temporal decorrelation but as well the *surface displacement rate plays* a significant role for successful observations. In order to properly measure a differential phase, ambiguities have to be avoided. This is the case, for instance, when the LOS-displacement at neighboring pixels exceeds $\lambda/4$ in-between two acquisitions. Here, a sampling interval below the $\lambda/4$ line should be defined in order to retrieve reliable results, as illustrated in Figure 14. However, when fringe visibility is high, displacement beyond the $\lambda/4$ line can be determined accurately when phases are unwrapped spatially as schematically shown in Figure 8. In either case, the confirmation of an absence of any ambiguities by an independent survey method with accuracy below the radar wavelength (λ) will constrain the results.

(d) The angle between the radar look direction and the displacement vectors (k in Figure 14) determines the sensitivity of the instrument to measure the displacement. Usually, in order to maximize this variable, the *look vector of the radar* needs to be as parallel to the displacement vector as possible (Figure 14). Alternatively, simultaneous interferometric observations from two observation sites yield modeled 3D-vectors if further assumptions are considered (e.g. surface parallel flow). In optimal cases, a real 3D displacement field can be measured where three instruments are arranged in rectangular observation geometry. Such a configuration yields 3D data for those segments only which are visible from each observation site. This would require a special terrain configuration such as a steep mountainous landscape with opposite valley flanks or open pit mines.

(e) The area undergoing displacement has to fulfill *minimum and maximum size constraints* if the goal is to measure displacement with conventional interferometric techniques. Here, a minimum size of several pixels in range and azimuth is required for the distinction between phase noise and real displacement. The spatial resolution of the radar image can then be determined with support of Figures 3 and 14. In addition, effects on the backscatter signal that depend on the SNR have to be considered. Usually, the SNR is a function of the system's performance and the radar-footprint. SNR usually decreases with range distance and local incidence angle (i in Figure 14). A trade-off therefore has to be made between ground-range resolution and SNR. A high SNR should be favored.
When the signals of coherent targets are processed, a single (point) scatterer can be tracked. However, the deformed area should consist of several targets in order to obtain sufficient control about the area undergoing displacement, and to increase the robustness of the statistics.
Radar interferometers are capable of measuring a relative displacement field only. Therefore surveys of regions where deformation occurs over very large areas (as is the case for regional subsidence, tidal processes and tectonic deformation) may yield non-conclusive results, mainly because the displacement signature of those processes cannot be separated from atmospheric and/or topographic effects without independent observations.

(f) *Atmospheric effects* induce significant phase shifts especially in the high frequency radar bands such as Ku and X. Turbulent atmospheric phase is a common phenomenon in alpine environments and is most often induced by differences in solar illumination. These effects can have a similar appearance in the acquired images as a displacement pattern. The differentiation between the signals derived from these mechanisms in a single interferogram is usually not possible without a priori information about the spatial extent of the deformed area. Effects related to atmospheric perturbations increase with range distance and become stronger with decreasing radar azimuth resolution. While atmospheric phase-shifts that depend on atmospheric range- and/or topographic height can be easily subtracted from the interferograms either with classic 2D interferometry approaches or point-based methods, these corrections are much more difficult to perform for images that were retrieved under turbulent atmospheric conditions. In cases where the use of lower radar-frequencies (C- to L-band) does not provide a viable alternative because of a loss of precision or resolution, the best strategy is to avoid turbulent conditions. This is usually the case during night or cloudy but stable weather conditions. Alternatively, interferogram averaging may lead to a reduction of phase shifts induced by turbulence in the atmosphere, but this requires a sufficient number of independent observations.
If continuous monitoring with combined alarming needs to be done under such conditions, warning thresholds have to be set accordingly so as to avoid false alarms. False alarms may occur due to errors associated with misinterpretation of atmospheric phase shifts. For an independent quality control of the displacement data, other measuring systems should be used to allow a redundant verification of processing results.

(g) Technical points and surveying strategies are mostly hardware related. Questions regarding the need of a stable (artificial) monument, transportability or portability are solved in different ways for different systems. Solutions range from setup on pickups or trailers, massive rectangular concrete monuments, measurement pillars or above a single marking ground point. Other technical aspects such as weather-proof casings, windstability, power-supply and communication interfaces for remote data and control access are provided by some manufacturers.

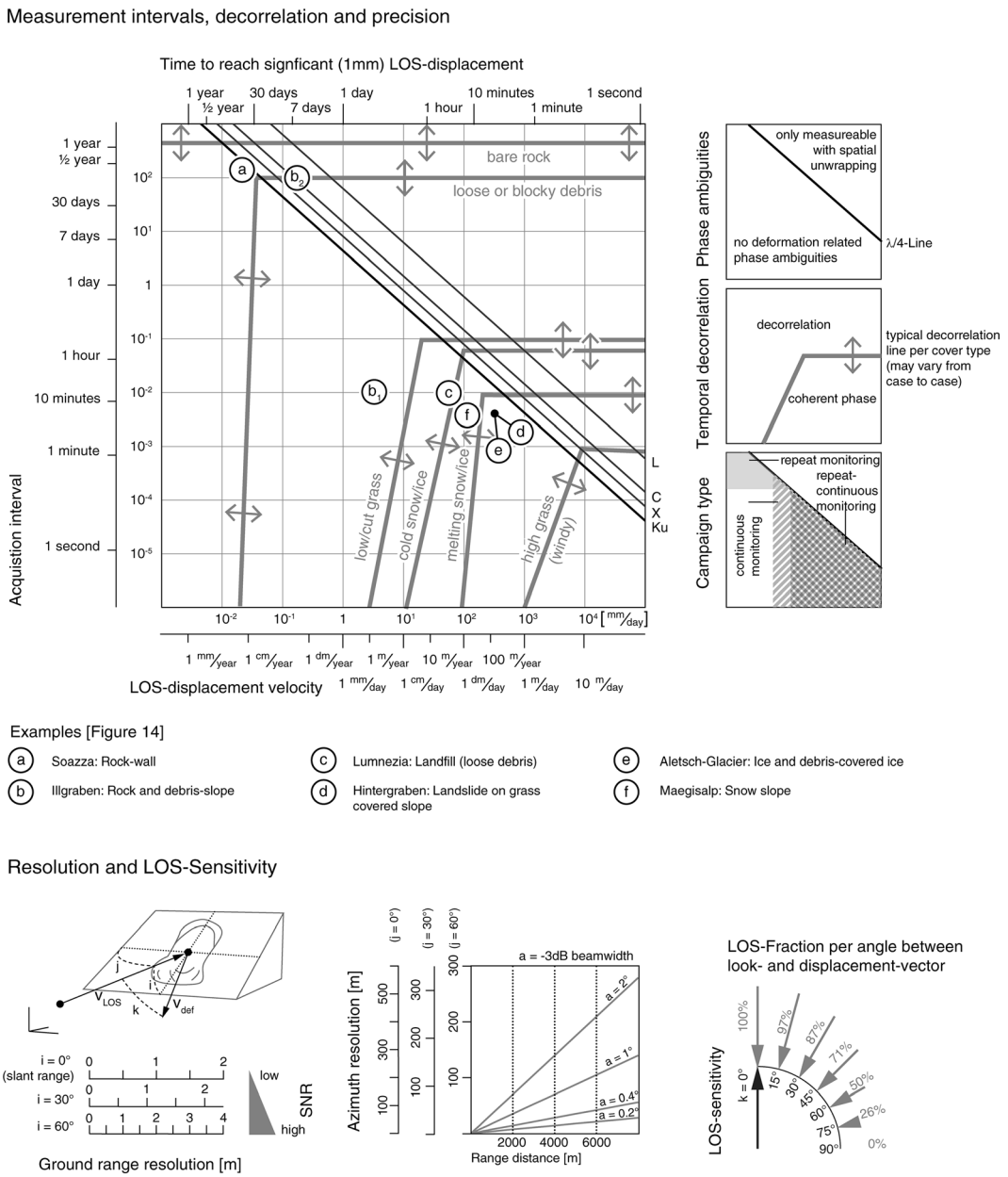

Figure 14. Decision aid for the planning of deformation measurements with terrestrial radar interferometry (TRI). Determination of measurement intervals has to be done by estimation of decorrelation times based on the surface cover in the target area. Coherent phase must be present. To avoid phase ambiguities due to fast deformation, measurement intervals have to be set best below the $\lambda/4$ line for the used wavelengths. Campaigns above this line requires spatial phase unwrapping. The examples from Figure 13 are plotted in the decision diagram.

A conclusive diagram illustrating the applicability and the performance of the planned campaign is presented in Figure 14 along with a presentation of the main limitations stated in points (a)–(g). Examples for targets with different surface properties are given in Figure 13. They have been surveyed with the Type-II interferometer GPRI. The corresponding sites within the decision diagram are indicated with the example numbers in Figure 14.

Following the strategy illustrated in Figure 14, the application of TRI for specific cases leads to interpretable results. The main graph considering decorrelation times, and the survey time needed to measure significant movement (1 mm) covers the majority of cases, but is not considered to be complete. Furthermore, the presented decorrelation times base on empiric observations of a real aperture Ku-band sensor (GPRI). Values for other sensors, especially C- to L-band sensors may vary significantly.

Conclusion and Outlook

Previous studies have shown that TRI is a tool with high potential for the detection and quantification of surface displacements. It has been possible to quantify a variety of geological geomorphological and glaciological processes and displacement mechanisms, where displacement rates span the entire spectrum from a very slow movement in rock-walls to very fast slip recorded by landslide surfaces or glaciers.

Decorrelation was identified as a major limiting factor for the successful application of TRI. The empirically derived temporal decorrelation times support the planning and execution of measurement campaigns. Considerations of decorrelation and displacement rates for different surface cover types are summarized as a graphical representation in Figure 14. This illustration also displays the expected resolutions for radar images and LOS-sensitivities.

As a final decision in the campaign planning, the type and repetition rate of the acquisitions has to be defined. In general, three main campaign types have been used in the past:

(i) Repeat-interferometry including non-interferometric methods
(ii) Short time continuous interferometry
(iii) Continuous interferometry.

(i) Repeat campaigns are suitable if the goal is to measure very slow displacement processes in highly coherent areas, such as rock wall displacements. Interferograms can be generated for scans retrieved days, weeks or even years apart. In either case, precise repositioning of the instrument (in 3D space) to a fixed measurement position must be achieved in order to minimize phase effects by a spatial offset of the instrument. Alternatively to the interferometric approach, intensity tracking on artificial reflectors may also reveal centimeter scale displacement.
(ii) Continuous interferometry over a short time can be applied to areas where the surfaces experience high displacement velocities, and where significant movement needs to be detected during several hours up to a few days. After a single campaign, the instantaneous velocity can be measured. The campaign can then be repeated after a longer time span. The instantaneous velocity measured during this second campaign can then be used for comparison. In addition, an interferogram covering a longer time interval between the two single campaigns eventually reveals slower movements, or allows mapping of the aerial extents where fast movements have occurred through the consideration of low coherence patches.
(iii) Continuous interferometric monitoring may require substantial installation efforts. Infrastructure such as weather shelter, long-term power-supply and data-transfer may be necessary, but it will add significant value to the monitoring of hazards where a high risk is recognized.

Over the past decade, the developments in the field of TRI have mainly been driven by needs related to real-time data-processing and mid- to long-term monitoring of unstable slopes. Environments with little vegetation or lack of snow cover have favorably been monitored in the past, since the success-rate regarding decorrelation effects is highest (Figure 14). Nevertheless, the limits of operations have been shifted towards surveying 'difficult to measure' scatterers parallel with improvements in the sensor design. For instance it is now possible to measure grass- and snow-slopes and glacier ice with coherent phases, yielding new quantitative insights in the process dynamics.

Finally, the technique offers new possibilities for early detection of surface movement because displacement of large areas can be measured with high precision, and the instrumentation can be operated remotely in difficult or dangerous to access terrain.

References

Abellán A, Jaboyedoff M, Oppikofer T, Vilaplana JM. 2009. Detection of millimetric deformation using a terrestrial laser scanner: experiment and application to a rockfall event. *Natural Hazards and Earth System Science* **9**: 365–372. DOI: 10.5194/nhess-9-365-2009

Agliardi F, Crosta G, Meloni F, Valle C, Rivolta C. 2013. Structurally-controlled instability, damage and slope failure in a porphyry rock mass. *Tectonophysics* **605**: 34–47. DOI: 10.1016/j.tecto.2013.05.033

Aguasca A, Broquetas A, Mallorqui J, Fabregas X. 2004. A solid state L to X-band flexible ground-based SAR system for continuous monitoring applications. *International Geoscience and Remote Sensing Symposium Proceedings* **2**: 757–760. DOI: 10.1109/IGARSS.2004.1368512

Bamler R, Hartl P. 1998. Synthetic aperture radar interferometry. *Inverse Problems* **14**(4): R1. DOI: 10.1088/0266–5611/14/4/001

Barla G, Antolini F, Barla M, Mensi E, Piovano G. 2010. Monitoring of the Beauregard landslide (Aosta Valley, Italy) using advanced and conventional techniques. *Engineering Geology* **116**: 218–235. DOI: 10.1016/j.enggeo.2010.09.004

Bennett G, Molnar P, Eisenbeiss H, McArdell B. 2012. Erosional power in the Swiss Alps: characterization of slope failure in the Illgraben. *Earth Surface Processes and Landforms* **37**: 1627–1640. DOI: 10.1002/esp.3263

Berardino P, Fornaro G, Lanari R, Sansosti E. 2002. A new algorithm for surface deformation monitoring based on small baseline differential SAR interferograms. *IEEE Transactions on Geoscience and Remote Sensing* **40**: 2375–2383. DOI: 10.1109/TGRS.2002.803792

Buckley SJ, Howell J, Enge H, Kurz T. 2008. Terrestrial laser scanning in geology: data acquisition, processing and accuracy considerations. *Journal of the Geological Society* **165**: 625–638. DOI: 10.1144/0016-76492007-100

Caduff R, Rieke-Zapp D. 2014. Registration and visualisation of deformation maps from terrestrial radar-interferometry using photogrammetry and structure from motion. *The Photogrammetric Record* **29**: 167–186. DOI: 10.1111/phor.12058

Caduff R, Strozzi T, Wiesmann A. 2013. Erfolgreicher Einsatz terrestrischer Radar–Interferometrie zur flächenhaften Vermessung von ausserordentlichen Hangrutschungsbewegungen im Gebiet Hintergraben/OW. *Swiss Bulletin für Angewandte Geologie* **18**: 129–138.

Caduff R, Kos A, Schlunegger F, McArdell B, Wiesmann A. 2014. terrestrial radar interferometric measurement of hillslope deformation and atmospheric disturbances in the Illgraben debris-flow catchment, Switzerland. *Geoscience and Remote Sensing Letters* **11**: 434–438. DOI: 10.1109/LGRS.2013.2264564

Calabro MD, Schmidt DA, Roering JJ. 2010. An examination of seasonal deformation at the Portuguese Bend landslide, southern California, using radar interferometry. *Journal of Geophysical Research, Earth Surface* **115**: F02020.

Catani F, Farina P, Moretti S, Nico G, Strozzi T. 2005. On the application of SAR interferometry to geomorphological studies: estimation of landform attributes and mass movements. *Geomorphology* **66**: 119–131.

Colesanti C, Wasowski J. 2006. Investigating landslides with space-borne synthetic aperture radar (SAR) interferometry. *Engineering Geology* **88**: 173–199. DOI: 10.1016/j.enggeo.2006.09.013

Colesanti C, Ferretti A, Novali F, Prati C, Rocca F. 2003. SAR monitoring of progressive and seasonal ground deformation using the permanent scatterers technique. *IEEE Transactions on Geoscience and Remote Sensing* **41**: 1685–1701. DOI: 10.1109/TGRS.2003.813278

Crosetto M, Monserrat O, Luzi G, Cuevas-González M, Devanthéry N. 2014a. Discontinuous GBSAR deformation monitoring. *ISPRS Journal of Photogrammetry and Remote Sensing* **93**: 136–141.

Crosetto M, Monserrat O, Luzi G, Cuevas-Gonzalez M, Devanthery N. 2014b. A noninterferometric procedure for deformation measurement using GB-SAR imagery. *Geoscience and Remote Sensing Letters, IEEE* **11**: 34–38.

Crosta G, DiPrisco C, Frattini P, Frigerio G, Castellanza R, Agliardi F. 2013. Chasing a complete understanding of the triggering mechanisms of a large rapidly evolving rockslide. *Landslides* **11**: 747–764. DOI: 10.1007/s10346-013-0433-1

Del Ventisette C, Casagli N, Fortuny-Guasch J, Tarchi D. 2011a. Ruinon landslide (Valfurva, Italy) activity in relation to rainfall by means of GBInSAR monitoring. *Landslides* **9**: 497–509. DOI: 10.1007/s10346-011-0307-3

Del Ventisette C, Intrieri E, Luzi G, Casagli N, Fanti R, Leva D. 2011b. Using ground based radar interferometry during emergency: the case of the A3 motorway (Calabria Region, Italy) threatened by a landslide. *Natural Hazards and Earth System Science* **11**: 2483–2495. DOI: 10.5194/nhess-11-2483-2011

Delaloye R, Lambiel C, Lugon R, Raetzo H, Strozzi T. 2007. Typical ERS InSAR signature of slope movements in a periglacial mountain environment (Swiss Alps). *Proceedings, Envisat Symposium*, Montreux Switzerland.

Dellepiane S, Bo G, Monni S, Buck C. 2000. SAR images and interferometric coherence for flood monitoring. *Proceedings, Geoscience and Remote Sensing Symposium, IGARSS 2000*. IEEE International: New York; 2608–2610.

Dixon TH, Voytenko D, Lembke C, DeLaPeña S, Howat I, Gourmelen N, Werner C, Oddsson B. 2012. Emerging technology monitors ice-sea interface at outlet glaciers. *Eos, Transactions American Geophysical Union* **93**: 497–498. DOI: 10.1029/2012EO480001

Dunnicliff J. 1993. Geotechnical Instrumentation for Monitoring Field Performance. John Wiley & Sons: Chichester.

Eberhardt E, Watson A, Loew S. 2008. Improving the interpretation of slope monitoring and early warning data through better understanding of complex deep-seated landslide failure mechanisms. In Landslides and Engineered Slopes: From the Past to the Future, Chen Z, Zhang J, Li Z, Wu F, Ho K (eds). Taylor & Francis: London; 39–51.

Engdahl M, Hyyppä J. 2003. Land-cover classification using multitemporal ERS-1/2 InSAR data. *IEEE Transactions on Geoscience and Remote Sensing* **41**: 1620–1628.

Fabregas X, Iglesias R, Aguasca A. 2012. A new approach for atmospheric phase screen compensation in ground-based SAR over areas with steep topography. *Proceedings, 9th European Conference on Synthetic Aperture Radar*, 12–15.

Ferretti A, Prati C, Rocca F. 2001. Permanent scatterers in SAR interferometry. *IEEE Transactions on Geoscience and Remote Sensing* **39**: 8–20. DOI: 10.1109/36.898661

Gigli G, Fanti R, Canuti P, Casagli N. 2011. Integration of advanced monitoring and numerical modeling techniques for the complete risk scenario analysis of rockslides: the case of Mt. Beni (Florence, Italy). *Engineering Geology* **120**: 48–59. DOI: 10.1016/j.enggeo.2011.03.017

Gischig V, Loew S, Kos A, Moore JR, Raetzo H, Lemy F. 2009. Identification of active release planes using ground-based differential InSAR at the Randa rock slope instability, Switzerland. *Natural Hazards and Earth System Science* **9**: 2027–2038. DOI: 10.5194/nhess-9-2027-2009

Goldstein RM. 1995. Atmospheric limitations to repeat–track radar interferometry. *Geophysical Research Letters* **22**: 2517–2520. DOI: 10.1029/95GL02475

Goldstein RM, Werner CL. 1998. Radar interferogram filtering for geophysical applications. *Geophysical Research Letters* **25**: 4035–4038. DOI: 10.1029/1998GL900033

Goldstein RM, Zebker HA, Werner CL. 1988. Satellite radar interferometry: two-dimensional phase unwrapping. *Radio Science* **23**: 713–720. DOI: 10.1029/RS023i004p00713

Hanssen RF. 2001. Radar Interferometry: Data Interpretation and Error Analysis, vol. **2**. Springer: Berlin.

Harries NJ, Noon D, Rowley K. 2006. Case studies of slope stability radar used in open cut mines. In Stability of Rock Slopes in Open Pit Mining and Civil Engineering Situations. Southern African Institute of Mining and Metallurgy Symposium Series S44, Cape Town; 335–342.

Harries NJ, Noon D, Pritchett H, Bates D. 2009. Slope stability radar for managing rock fall risks in open cut mines. *ROCKENG09: Proceedings of the 3rd CANUS Rock Mechanics Symposium*.

Herrera G, Fernández-Merodo J, Mulas J, Pastor M, Luzi G, Monserrat O. 2009. A landslide forecasting model using ground based SAR data: the Portalet case study. *Engineering Geology* **105**: 220–230. DOI: 10.1016/j.enggeo.2009.02.009

Herrera G, Notti D, García-Davalillo J, Mora O, Cooksley G, Sánchez M, Arnaud A, Crosetto M. 2011. Analysis with C- and X-band satellite SAR data of the Portalet landslide area. *Landslides* **8**: 195–206.

Hooper A, Zebker HA. 2007. Phase unwrapping in three dimensions with application to InSAR time series. *Journal of the Optical Society of America, A: Optics, Image Science, and Vision* **24**: 2737–2747. DOI: 10.1364/JOSAA.24.002737

Hooper A, Segall P, Zebker H. 2007. Persistent scatterer interferometric synthetic aperture radar for crustal deformation analysis, with application to Volcán Alcedo, Galápagos. *Journal of Geophysical Research* **112**: B07407. DOI: 10.1029/2006JB004763

Hooper A, Bekaert D, Spaans K, Arıkan M. 2012. Recent advances in SAR interferometry time series analysis for measuring crustal deformation. *Tectonophysics* **514–517**: 1–13.

Hovius N, Stark CP, Allen PA. 1997. Sediment flux from a mountain belt derived by landslide mapping. *Geology* **25**: 231–234. DOI: 10.1130/0091-7613(1997)025<0231:SFFAMB>2.3.CO;2

Huang L, Li Z. 2011. Comparison of SAR and optical data in deriving glacier velocity with feature tracking. *International Journal of Remote Sensing* **32**: 2681–2698.

Intrieri E, Traglia FD, Ventisette CD, Gigli G, Mugnai F, Luzi G, Casagli N. 2013. Flank instability of Stromboli volcano (Aeolian Islands, Southern Italy): integration of GB-InSAR and geomorphological observations. *Geomorphology* **201**: 60–69. DOI: 10.1016/j.geomorph.2013.06.007

Jaboyedoff M, Oppikofer T, Abellán A, Derron MH, Loye A, Metzger R, Pedrazzini A. 2012. Use of LIDAR in landslide investigations: a review. *Natural Hazards* **61**: 5–28.

James MR, Robson S. 2012. Straightforward reconstruction of 3D surfaces and topography with a camera: accuracy and geoscience application. *Journal of Geophysical Research* **117**: F03017.

Jung H, Lu Z, Won JS, Poland M, Miklius A. 2011. Mapping three-dimensional surface deformation by combining multiple-aperture interferometry and conventional interferometry: application to the June 2007 eruption of Kilauea Volcano, Hawaii. *Geoscience and Remote Sensing Letters, IEEE* **8**: 34–38.

Kääb A. 2008. Remote sensing of permafrost-related problems and hazards. *Permafrost and Periglacial Processes* **19**: 107–136.

Kääb A, Girod L, Berthling I. 2014. Surface kinematics of periglacial sorted circles using structure-from-motion technology. *The Cryosphere* **8**: 1041–1056.

Kobayashi T. 2014. Remarkable ground uplift and reverse fault ruptures for the 2013 Bohol earthquake (Mw 7.1), Philippines, revealed by SAR pixel offset analysis. *Geoscience Letters* **1**: 1–10.

Korup O, Clague JJ. 2009. Natural hazards, extreme events, and mountain topography. *Quaternary Science Reviews* **28**: 977–990. DOI: 10.1016/j.quascirev.2009.02.021

Kos A, Lunghi A, Conforti A, Tompkinson W, Strozzi T, Wiesmann A. 2011. Integration of terrestrial lidar and ground-based radar interferometry for monitoring rock slopes following blast mitigation. In: Proceedings of the 11th IAEG Congress. Auckland, New Zealand, 5–10 September 2010. 8 Pages.

Kos A, Strozzi T, Stockmann R, Wiesmann A, Werner C. 2013. Detection and characterization of rock slope instabilities using a portable radar interferometer (GPRI). In Landslide Science and Practice, Margottini C, Canuti P, Sassa K (eds). Springer: Berlin; 325–329.

Kristensen L, Rivolta C, Dehls J, Blickra LH. 2013. GB InSAR measurement at the Aknes rockslide, Norway. *Italian Journal of Engineering Geology and Environment – Book Series* **6**: 339–348.

Leva D, Nico G, Tarchi D, Fortuny-Guasch J, Sieber A. 2003. Temporal analysis of a landslide by means of a ground-based SAR Interferometer. *IEEE Transactions on Geoscience and Remote Sensing* **41**: 745–752. DOI: 10.1109/TGRS.2003.808902

Li Z, Muller JP, Cross P, Fielding EJ. 2005. Interferometric synthetic aperture radar (InSAR) atmospheric correction: GPS, moderate resolution imaging spectroradiometer (MODIS), and InSAR integration. *Journal of Geophysical Research* **110**: B03410. DOI: 10.1029/2004JB003446

Lowry B, Gomez F, Zhou W, Mooney M, Held B, Grasmick J. 2013. High resolution displacement monitoring of a slow velocity landslide using ground based radar interferometry. *Engineering Geology* **166**: 160–169. DOI: 10.1016/j.enggeo.2013.07.007

Lundgren P, Casu F, Manzo M, Pepe A, Berardino A, Sansosti E, Lanari R. 2004. Gravity and magma induced spreading of Mount Etna volcano revealed by satellite radar interferometry. *Geophysical Research Letters* **31**: 1–4.

Luzi G. 2010. Ground based SAR interferometry: a novel tool for geoscience. In: Imperatore P, Riccio D (eds.). *Geoscience and Remote Sensing New Achievements*, Intech 2010. 1–26. DOI: 10.5772/9090

Luzi G, Pieraccini M, Mecatti D, Noferini L, Guidi G, Moia F, Atzeni C. 2004. Ground-based radar interferometry for landslides monitoring: atmospheric and instrumental decorrelation sources on experimental data. *IEEE Transactions on Geoscience and Remote Sensing* **42**: 2454–2466. DOI: 10.1109/TGRS.2004.836792

Luzi G, Pieraccini M, Mecatti D, Noferini L, Macaluso G, Tamburini A, Atzeni C. 2007. Monitoring of an alpine glacier by means of ground-based SAR interferometry. *Geoscience and Remote Sensing Letters* **4**: 495–499. DOI: 10.1109/LGRS.2007.898282

Luzi G, Noferini L, Mecatti D, Macaluso G, Pieraccini M, Atzeni C, Schaffhauser A, Fromm R, Nagler T. 2009. Using a ground-based

SAR interferometer and a terrestrial laser scanner to monitor a snow-covered slope: results from an experimental data collection in Tyrol (Austria). *IEEE Transactions on Geoscience and Remote Sensing* **47**: 382–393. DOI: 10.1109/TGRS.2008.2009994

Magnusson E, Rott H, Björnsson H, Palsson F. 2007. The impact of jökulhlaups on basal sliding observed by SAR interferometry on Vatnajökull, Iceland. *Journal of Glaciology* **53**: 232–240.

Martinez-Vazquez A, Fortuny-Guasch J. 2006. Feasibility of snow avalanche volume retrieval by GB-SAR imagery. *Proceedings, International Geoscience and Remote Sensing Symposium, IGARSS 2006*, 743–746. DOI: 10.1109/IGARSS.2006.191

Martinez-Vazquez A, Fortuny-Guasch J. 2008. A GB-SAR processor for snow avalanche identification. *IEEE Transactions on Geoscience and Remote Sensing* **46**: 3948–3956. DOI: 10.1109/TGRS.2008.2001387

Massonnet D, Feigl KL. 1998. Radar interferometry and its application to changes in the Earth's surface. *Reviews of Geophysics* **36**: 441–500.

Massonnet D, Rossi M, Carmona C, Adragna F, Peltzer G, Feigl K, Rabaute T. 1993. The displacement field of the Landers earthquake mapped by radar interferometry. *Nature* **364**: 138–142.

Mazzanti P, Brunetti A. 2010. Assessing rockfall susceptibility by terrestrial SAR interferometry. *Mountain Risks*: *Bringing Science to Society, Proceedings of the International Conference, CERG Editions*, 24–26 November 2010, Florence, Italy; 109–114.

Michoud C, Bazin S, Blikra LH, Derron, MH, Jaboyedoff M. 2013. Experiences from site-specific landslide early warning systems. *Natural Hazards and Earth System Science* **13**: 2659–2673.

Mohr JJ, Reeh N, Madsen SN. 1998. Three-dimensional glacial flow and surface elevation measured with radar interferometry. *Nature* **391**: 273–276. DOI: 10.1038/34635

Monserrat O, Moya J, Luzi G, Crosetto M, Gili J, Corominas J. 2013. Non-interferometric GB-SAR measurement: application to the Vallcebre landslide (eastern Pyrenees, Spain). *Natural Hazards and Earth System Sciences* **13**: 1873–1887.

Monserrat O, Crosetto M, Luzi G. 2014. A review of ground-based SAR interferometry for deformation measurement. *ISPRS Journal of Photogrammetry and Remote Sensing* **93**: 40–48.

Nagler T, Rott H, Hetzenecker M, Scharrer K, Magnusson E, Floricioiu D, Notarnicola C. 2012. Retrieval of 3D-glacier movement by high resolution X-band SAR data. *Proceedings, IEEE International Geoscience and Remote Sensing Symposium* (*IGARSS*); 3233–3236.

Nico G, Leva D, Fortuny-Guasch J, Antonello G, Tarchi D. 2005. Generation of digital terrain models with a ground-based SAR system. *IEEE Transactions on Geoscience and Remote Sensing* **43**: 45–49. DOI: 10.1109/TGRS.2004.838354

Noferini L, Pieraccini M, Mecatti D, Luzi G, Atzeni C, Tamburini A, Broccolato M. 2005. Permanent scatterers analysis for atmospheric correction in ground-based SAR interferometry. *IEEE Transactions on Geoscience and Remote Sensing* **43**: 1459–1471.

Noferini L, Pieraccini M, Mecatti D, Macaluso G, Luzi G, Atzeni C. 2007. DEM by ground-based SAR interferometry. *Geoscience and Remote Sensing Letters, IEEE* **4**: 659–663.

Noferini L, Takayama T, Pieraccini M, Mecatti D, Macaluso G, Luzi G, Atzeni C. 2008. Analysis of ground-based SAR data with diverse temporal baselines. *IEEE Transactions on Geoscience and Remote Sensing* **46**: 1614–1623. DOI: 10.1109/TGRS.2008.916216

Noferini L, Mecatti D, Macaluso G, Pieraccini M, Atzeni C. 2009. Monitoring of Belvedere Glacier using a wide angle GB-SAR interferometer. *Journal of Applied Geophysics* **68**: 289–293. DOI: 10.1016/j.jappgeo.2009.02.004

Osasan KD. 2012. Open-cast Mine Slope Deformation and Failure Mechanisms Interpreted from Slope Radar Monitoring. PhD Thesis, Faculty of Engineering and the Built Environment, University of the Witwatersrand, Johannesburg.

Paar G, Huber NB, Bauer A, Avian M, Reiterer A. 2012. Vision-based terrestrial surface monitoring. In Terrigenous Mass Movements. Springer: Berlin; 283–348.

Pipia L, Aguasca A, Fabregas X, Mallorqui J, Lopez-Martinez C, Marturia J. 2007. Mining induced subsidence monitoring in urban areas with a ground-based SAR. *Proceedings, Urban Remote Sensing Joint Event*, 1–5. DOI: 10.1109/URS.2007.371881

Pipia L, Fabregas X, Aguasca A, Lopez-Martinez C. 2008. Atmospheric artifact compensation in ground-based DInSAR applications. *Geoscience and Remote Sensing Letters* **5**: 88–92. DOI: 10.1109/LGRS.2007.908364

Reeves BA, Stickley G, Noon D, Longstaff ID. 2000. Developments in monitoring mine slope stability using radar interferometry. *International Geoscience and Remote Sensing Symposium, IGARSS* **5**: 2325–2327. DOI: 10.1109/IGARSS.2000.858397

Reeves B, Noon DA, Stickley GF, Longstaff D. 2001. Slope stability radar for monitoring mine walls. *Proceedings of SPIE*; 57–67. DOI: 10.1117/12.450188

Rieke-Zapp D, Nearing MA. 2005. Digital close range photogrammetry for measurement of soil erosion. *The Photogrammetric Record* **20**: 69–87. DOI: 10.1111/j.1477-9730.2005.00305.x

Riesen P, Strozzi T, Bauder A, Wiesmann A, Funk M. 2011. Short-term surface ice motion variations measured with a ground-based portable real aperture radar interferometer. *Journal of Glaciology* **57**: 53–60. DOI: 10.3189/002214311795306718

Rödelsperger S. 2011. Real-time Processing of Ground Based Synthetic Aperture Radar (GB-SAR) Measurements. Technische Universität Darmstadt, Fachbereich Bauingenieurwesen und Geodäsie, Darmstadt.

Rödelsperger S, Läufer G, Gerstenecker C, Becker M. 2010a. Monitoring of displacements with ground-based microwave interferometry: IBIS-S and IBIS-L. *Journal of Applied Geodesy* **4**: 41–54. DOI: 10.1515/jag.2010.005

Rödelsperger S, Becker M, Gerstenecker C, Läufer G, Schilling K, Steineck D. 2010b. Digital elevation model with the ground-based SAR IBIS-L as basis for volcanic deformation monitoring. *Journal of Geodynamics* **49**: 241–246. DOI: 10.1016/j.jog.2009.10.009

Rödelsperger S, Coccia A, Vicente D, Meta A. 2012. Introduction to the new metasensing ground-based SAR: technical description and data analysis. *Proceedings, Geoscience and Remote Sensing Symposium, IGARSS 2012*; 4790–4792. DOI: 10.1109/IGARSS.2012.6352542

Rödelsperger S, Coccia A, Vicente D, Trampuz C, Meta A. 2013. The novel FastGBSAR sensor: deformation monitoring for dike failure prediction. *Proceedings, Asia-Pacific Conference on Synthetic Aperture Radar* (*APSAR*), 23–27 September 2013; 420–423.

Roering JJ, Stimely LL, Mackey BH, Schmidt DA. 2009. Using DInSAR, airborne LiDAR, and archival air photos to quantify landsliding and sediment transport. *Geophysical Research Letters* **36**: L19402.

Rosen P, Hensley S, Joughin I, Li F, Madsen S, Rodriguez E, Goldstein R. 2000. Synthetic aperture radar interferometry. *Proceedings of the IEEE* **88**: 333–382. DOI: 10.1109/5.838084

Rott H, Nagler T. 2006. The contribution of radar interferometry to the assessment of landslide hazards. *Advances in Space Research* **37**: 710–719.

Rudolf H, Leva D, Tarchi D, Sieber A. 1999. A mobile and versatile SAR system. *Proceedings, International Geoscience and Remote Sensing Symposium, IGARSS 99*; 592–594. DOI: 10.1109/IGARSS.1999.773575

Santoro M, Wegmüller U, Askne J. 2010. Signatures of ERS – Envisat interferometric SAR coherence and phase of short vegetation: an analysis in the case of maize fields. *IEEE Transactions on Geoscience and Remote Sensing* **48**: 1702–1713. DOI: 10.1109/TGRS.2009.2034257

Schuerch P, Densmore AL, McArdell BW, Molnar P. 2006. The influence of landsliding on sediment supply and channel change in a steep mountain catchment. *Geomorphology* **78**: 222–235. DOI: 10.1016/j.geomorph.2006.01.025

Schulz WH, Kean JW, Wang G. 2009. Landslide movement in southwest Colorado triggered by atmospheric tides. *Nature Geoscience* **2**: 863–866. DOI: 10.1038/ngeo659

Severin J, Eberhardt E, Leoni L, Fortin S. 2011. Use of ground-based synthetic aperture radar to investigate complex 3-D pit slope kinematics. *Proceedings of the International Symposium on Rock Slope Stability in Open Pit Mining and Civil Engineering*, 18–21 September 2011, Vancouver, Canada.

Smith G, Askne J. 2001. Clear-cut detection using ERS interferometry. *International Journal of Remote Sensing* **22**: 3651–3664.

Springman SM, Arenson LU, Yamamoto Y, Maurer H, Kos A, Buchli T, Derungs, G. 2012. Multidisciplinary investigations on three rock-glaciers in the Swiss Alps: legacies and future perspectives. *Geografiska Annaler: Series A, Physical Geography* **94**: 215–243. DOI: 10.1111/j.1468-0459.2012.00464.x

Strozzi T, Dammert P, Wegmüller U, Martinez JM, Askne J, Beaudoin A, Hallikainen M. 2000. Landuse mapping with ERS SAR interferometry.

IEEE Transactions on Geoscience and Remote Sensing **38**: 766–775. DOI: 10.1109/36.842005

Strozzi T, Wegmüller U, Tosi L, Bitelli G, Spreckels V. 2001. Land subsidence monitoring with differential SAR interferometry. *Photogrammetric Engineering and Remote Sensing* **67**: 1261–1270.

Strozzi T, Farina P, Corsini A, Ambrosi C, Thüring M, Zilger J, Wiesmann A, Wegmüller U, Werner C. 2005. Survey and monitoring of landslide displacements by means of L-band satellite SAR interferometry. *Landslides* **2**: 193–201.

Strozzi T, Delaloye R, Raetzo H, Wegmüller U. 2009. Radar interferometric observations of destabilized rockglaciers. In Proceeding of Fringe 2009 Workshop, Lacoste-Francis H (ed.). 30 November–4 December 2009, ESRIN, Frascati, Italy. ESA Communications, European Space Agency.

Strozzi T, Werner C, Wiesmann A, Wegmüller U. 2011. Topography mapping with a portable real-aperture radar interferometer. *Geoscience and Remote Sensing Letters* **9**: 277–281. DOI: 10.1109/LGRS.2011.2166751

Tapete D, Casagli N, Luzi G, Fanti R, Gigli G, Leva D. 2013. Integrating radar and laser-based remote sensing techniques for monitoring structural deformation of archaeological monuments. *Journal of Archaeological Science* **40**: 176–189.

Tarchi D, Casagli N, Moretti S, Leva D, Sieber AJ. 2003. Monitoring landslide displacements by using ground-based synthetic aperture radar interferometry: application to the Ruinon landslide in the Italian Alps. *Journal of Geophysical Research* **108**: 2387. DOI: 10.1029/2002JB002204

Tarchi D, Antonello G, Casagli N, Farina P, Fortuny-Guasch J, Guerri L, Leva D. 2005. On the use of ground-based SAR interferometry for slope failure early warning: the Cortenova rock slide (Italy). In Landslides, Sassa K, Fukuoka H, Wang F, Wang G (eds). Springer: Berlin; 337–342.

Thut A. 2009. Geotechnische Messverfahren. Wiley-VCH Verlag: Weinheim; 653–717.

Tosi L, Teatini P, Strozzi T. 2013. Natural versus anthropogenic subsidence of Venice. *Scientific Reports* **3**: 403–417. DOI: 10.1038/srep02710

Travelletti J, Delacourt C, Allemand P, Malet JP, Schmittbuhl J, Toussaint R, Bastard M. 2012. Correlation of multi-temporal ground-based optical images for landslide monitoring: application, potential and limitations. *ISPRS Journal of Photogrammetry and Remote Sensing* **70**: 39–55.

Ulaby F, Moore R, Fung A. 1987. Microwave Remote Sensing Active and Passing Volume 2: Radar Remote Sensing and Surface Scattering and Emission Theory. Artech House: Boston, MA.

Usai S. 2002. A least-squares approach for long-term monitoring of deformations with differential SAR interferometry. *International Geoscience and Remote Sensing Symposium* **2**: 1247–1250. DOI: 10.1109/IGARSS.2002.1025903

Voytenko D, Dixon TH, Werner C, Gourmelen N, Howat IM, Tinder PC, Hooper A. 2012. Moniotoring a glacier in southeastern Iceland with the portable terrestrial radar interferometer. *Proceedings, International Geoscience and Remote Sensing Symposium*; 3230–3232. DOI: 10.1109/IGARSS.2012.6350736

Wangensteen B, Guðmundsson Á, Eiken T, Kääb A, Farbrot H, Etzelmüller B. 2006. Surface displacements and surface age estimates for creeping slope landforms in northern and eastern Iceland using digital photogrammetry. *Geomorphology* **80**: 59–79.

Wegmüller U, Werner C. 1995. SAR interferometric signatures of forest. *IEEE Transactions on Geoscience and Remote Sensing* **33**: 1153–1161.

Werner C, Strozzi T, Wegmüller U, Wiesmann A. 2002. SAR geocoding and multi-sensor image registration. *International Geoscience and Remote Sensing Symposium* **2**: 902–904. DOI: 10.1109/36.469479

Werner C, Wegmüller U, Strozzi T, Wiesmann A. 2003. Interferometric point target analysis for deformation mapping. *International Geoscience and Remote Sensing Symposium* **7**: 4362–4364. DOI: 10.1109/IGARSS.2003.1295516

Werner C, Strozzi T, Wiesmann A, Wegmüller U. 2008. A real-aperture radar for ground-based differential interferometry. *International Geoscience and Remote Sensing Symposium* **3**: 10–13. DOI: 10.1109/IGARSS.2008.4779320

Werner C, Wiesmann A, Strozzi T, Kos A, Caduff R, Wegmüller U. 2012. The GPRI multi-mode differential interferometric radar for ground-based observations. *Proceedings, 9th European Conference on Synthetic Aperture Radar*; 304–307.

Wiesmann A, Caduff R, Strozzi T, Papke J, Mätzler Ch. 2014. Monitoring of dynamic changed in alpine snow with terrestrial radar interferometry. *Proceedings, International Geoscience and Remote Sensing Symposium*.

Zebker HA, Villasenor J. 1992. Decorrelation in interferometric radar echoes. *IEEE Transactions on Geoscience and Remote Sensing* **30**: 950–959. DOI: 10.1109/36.175330

Zebker HA, Rosen PA, Hensley S. 1997. Atmospheric effects in interferometric synthetic aperture radar surface deformation and topographic maps. *Journal of Geophysical Research* **102**: 7547–7563. DOI: 10.1029/96JB03804